

This is a preprint of an article that has been submitted to Nature, and revised based on two rounds of peer review, but has yet to be formally accepted for publication.

1 **The longest-lived Pacific hotspots reveal a plume tail for the largest oceanic plateau**

2
3 J.G. Konter^{a†}, V.A. Finlayson^{a,b*}, K. Konrad^c, M.G. Jackson^d, A.A.P. Koppers^e, P. Wessel^{a†}, S.
4 Beethe^e, M. Bizimis^f, A. Alverson^g, C. Kelley^a

5 *^aDept. of Earth Sciences, School of Ocean and Earth Science and Technology, University of*
6 *Hawaii, Manoa, Honolulu, HI 96822, USA*

7 *^bDept. of Geology, University of Maryland, College Park, MD 20742, USA (*Corresponding*
8 *author; vfinlays@umd.edu)*

9 *^cDept. of Geoscience, University of Nevada Las Vegas, Las Vegas, NV, 89154, USA*

10 *^dDept. of Earth Science, University of California Santa Barbara, Santa Barbara, CA 93106, USA*

11 *^eCollege of Earth, Ocean and Atmospheric Sciences, Oregon State University, Corvallis, OR*
12 *97331, USA*

13 *^fSchool of the Earth, Ocean, and Environment, University of South Carolina, Columbia, SC,*
14 *29208, USA*

15 *^gDept. of Earth, Environmental and Planetary Sciences, Brown University, Providence, RI*
16 *02912, USA*

17 *[†]author deceased*

20 **Volcanic hotspots are thought to initially form by melting in an upwelling mantle plume head**
21 **followed by melting of the plume tail. Plate motion then generates an age progressive volcanic**
22 **track originating from a large igneous province and connecting to a presently active hotspot.**
23 **However, the most voluminous large igneous province, the ~120 Ma Ontong-Java Nui**
24 **Plateau (OJP-Nui) in the mid-Pacific, appears to lack such a volcanic track. Although the**
25 **Louisville hotspot track was originally proposed as a candidate, limited constraints for**
26 **Pacific absolute plate and plume motion prior to 80 Ma suggest a mismatch¹. Existing Pacific**
27 **models rely on age-distance data from the continuous Hawaii-Emperor and Louisville**
28 **volcanic tracks, but their seamounts older than ~80 Ma are now subducted, and elsewhere**
29 **on the Pacific plate only discontinuous and sparse seamount tracks can be found that formed**
30 **prior to 80 Ma²⁻⁷. These existing models require ~1,200 km of latitudinal motion for the**
31 **Louisville plume to also erupt the OJP-Nui¹, yet paleolatitude estimates from to ~70 Ma to**
32 **today remain within error of its present location^{8,9} and suggest that any major amount of**
33 **Louisville plume motion should precede that time. Here we provide evidence from**
34 **geochemistry and eruption ages⁹⁻¹⁴ demonstrating that Samoa and Rurutu-Arago are the**
35 **longest-lived Pacific hotspots that can be traced back to ~120 Ma (and older) in the West**
36 **Pacific where they subduct into the Mariana Trench. These newly defined tracks provide for**
37 **an alternative Pacific absolute plate motion model, with better constraints for a plate**
38 **rotation between 80-100 Ma, and allow us to establish Louisville as the missing volcanic track**
39 **for OJP-Nui without requiring major plume motion.**

40 Plume-fed hotspots exhibit age-progressive volcanic tracks that often originate from a large
41 igneous province (LIP), which marks a hotspot's inception¹⁵⁻¹⁸. Eruption of a LIP is thought to
42 correspond to the arrival of the head of a deeply-rooted mantle plume, causing extensive melting
43 in the upper mantle and unusually voluminous eruptions comprising the LIP^{3,19,20}. The Ontong-
44 Java Plateau (OJP; Fig. 1) once formed greater Ontong-Java Nui (OJP-Nui), together with the
45 Manihiki and Hikurangi plateaus²¹. Despite a proposed plume origin^{22,23}, there is no obvious age-
46 progressive volcanic track emerging from the plateau. Although the Louisville hotspot was
47 proposed to be related²⁴, later paleomagnetic and geochemistry data argued against a Louisville
48 hotspot connection with the OJP²⁵⁻²⁷. Recently obtained Louisville paleomagnetic latitudes are
49 constant within error up to ~70 Ma⁸, suggesting that any Louisville plume motion should precede
50 70 Ma. In that timeframe, existing absolute plate motion (APM) models require ~1,200 km of

51 plume motion to place Louisville and OJP in the same original eruptive location¹. However, more
52 recent geochemical data revealing similar Nd-Pb-Sr systematics between the main phase of the
53 OJP-Nui system and the Louisville Seamount track are permissive of the Louisville-OJP
54 connection²⁸ (Fig. 2). Additionally, here we show that the two longest-lived Pacific hotspot tracks
55 —Samoa and Rurutu-Arago^{9,14} (see below)—yield a new APM model that supports a genetic link
56 between the Louisville hotspot track and OJP-Nui, the largest LIP preserved in the geologic record.

57 Most existing Pacific APM models rely significantly on the Hawaii-Emperor and
58 Louisville hotspots back to 80 Ma, while unrelated discontinuous volcanic structures are used for
59 Pacific plate motion prior to 80 Ma^{2,3,7,18,29,30} (Fig. 1, Extended Data Fig. 1). These structures
60 include the Shatsky Rise, Hess Rise, Mid-Pacific Mountains, Line Islands, Lili‘uokalani
61 Seamounts, Musician Seamounts, Wake Seamounts, Marshall Islands, and Magellan Seamounts.
62 From these, the Mid-Pacific Mountains and Shatsky Rise erupted near all-ridge triple junctions,
63 while Hess Rise and Musicians Seamounts erupted near-ridge^{29–32} (Extended Data Fig. 2). Plume-
64 ridge interactions could significantly displace the upwelling mantle plume³³ such that resulting
65 plume motion is inadvertently included in the APM models. Moreover, the Line Islands lack a
66 clear age progression³⁴, the Musician Seamounts are complicated by overprinting of deformation-
67 related volcanism³³, and Shatsky Rise was recently suggested to be controlled by seafloor
68 spreading³⁵. In summary, all of these structures are unlikely to exclusively represent absolute plate
69 motion, yet the Wake, Marshall, and Magellan seamounts appear to be the only truly intra-plate
70 Pacific hotspots prior to 80 Ma (Extended Data Fig. 2). As we will demonstrate, they represent the
71 Cretaceous portions of two long-lived Pacific hotspots—Samoa and Rurutu-Arago—that can
72 extend Hawaii-Emperor and Louisville anchored Pacific APM models to the 80-120 Ma period.

73 The clearly defined Hawaii-Emperor and Louisville hotspot tracks provide a continuous
74 hotspot record for APM modeling back to approximately 80 Ma, where they subduct into the
75 Kamchatka and Tonga trenches, respectively^{8,36} (Fig. 1; Extended Data Fig. 1). However, changing
76 paleomagnetic latitudes³⁷, predictions of hotspot motion based on Indo-Atlantic hotspots³⁸, and
77 inter-hotspot differences in age progressions and distances^{9,39,40} all suggest relative motion
78 between these two plumes and the Pacific plate. Supporting this contention, models using global
79 mantle flow to predict plume motions have been argued to provide a better fit to the actual hotspot
80 tracks across ocean basins than fixed plume models⁶. The improved fit incorporating these

81 geodynamic models suggests that some hotspot tracks provide a combined record of plate motion
82 and plume motion^{3,5,18}, although fixed-hotspot models reproduce most tracks to first order.

83 On the Pacific plate, the Rurutu-Arago volcanic track—defined from young to old by the
84 Cook-Austral Islands, Tuvalu Islands, the Marshall Islands and Wake Seamounts—represents the
85 third long-lived hotspot in addition to Hawaii-Emperor and Louisville (Fig. 1). Changes in the
86 distance between these three hotspots from 60 to 50 Ma suggest that the Hawaii-Emperor hotspot
87 moved more significantly and mostly independently from both Louisville and Rurutu-Arago⁹.
88 However, more critical here is the fact that the Rurutu-Arago and Samoan hotspots can be traced
89 further back into the Cretaceous than Hawaii and Louisville. The older portions of the Rurutu-
90 Arago and Samoa hotspots both extend into the West Pacific, where tracing their tracks through
91 the high density of Cretaceous seamounts has required the mapping out of well-defined age
92 progressions combined with unique geochemical signatures^{4,12,14} (Fig. 1, Extended Data Fig. 7, 8).

93 To this end, we present new isotope geochemistry and, where possible, age determinations
94 from seamounts around Wake Island, a critical geological nexus that links the older (>80 Ma)
95 segment of the long-lived Rurutu-Arago hotspot track to the younger (< 80 Ma) portion originating
96 in the Cook-Austral Islands^{4,12,14,41,42}. We use this hotspot track, together with the long-lived
97 Samoan hotspot track, to generate a new APM stage pole between 80-100 Ma that resolves the
98 apparent disconnect between OJP-Nui and the Louisville hotspot.

99 The extreme and distinct hotspot compositions originating in the central Pacific⁴¹ have
100 generated clearly traceable hotspot tracks (Fig. 1, Extended Data Fig. 8). We reveal these tracks
101 by color coding (Fig. 1) based on the ⁸⁷Sr/⁸⁶Sr-¹⁴³Nd/¹⁴⁴Nd-²⁰⁶Pb/²⁰⁴Pb isotopic compositions of
102 lavas at each volcano along the hotspot tracks^{9-14,43,44}. In particular, high ²⁰⁶Pb/²⁰⁴Pb compositions
103 are an identifying feature of the Rurutu-Arago hotspot and can be traced back into the Western
104 Pacific along an age progression (blue, Fig. 1; Extended Data Fig. 8). However, north of the
105 Marshall Islands, a data gap in the Rurutu-Arago hotspot track separated these ≤80 Ma volcanoes
106 from the ≥100 Ma Wake Seamounts, complicating efforts to trace the Rurutu-Arago track prior to
107 80 Ma. Our recent sampling of seamounts around Wake Island fills this gap and Pb-Sr-Nd isotopic
108 compositions (Methods) of these samples match those of the rest of the Rurutu-Arago hotspot track
109 (Extended Data Fig. 8, Extended Data Fig. 9). We also present a new age of 91.3 Ma from a Wake

110 Island seamount (Supplemental Data Table 1, 3, Methods) that places it directly on the Rurutu-
111 Arago hotspot age progression (Extended Data Figure 8).

112 Further west, the Cretaceous Magellan seamounts also span the ~80-100 Ma age range⁴
113 and overlap with the Samoa hotspot in composition. Critically, the age and location of these
114 seamounts matches the predicted track of Samoa (Fig. 1; Extended Data Fig. 8) that, until now,
115 could be traced only from the present-day location near the northern terminus of the Tonga Trench
116 to ~25 Ma Alexa Bank, west of which the trace of the Samoan hotspot is lost in the Vitiaz Trench.
117 The predicted Samoan hotspot track passes through the OJP, where its large lithospheric
118 thickness²⁰ likely suppressed Samoan plume melting and volcanic construction⁴⁵. The predicted
119 hotspot therefore is expected to emerge on the north side of the OJP as 80-100 Ma volcanoes,
120 which is consistent with the age and location of the Magellan Seamounts. Further supporting a link
121 to the Samoan hotspot, the Magellan seamounts feature the same unique combination of
122 intermediate $^{206}\text{Pb}/^{204}\text{Pb}$ and extreme radiogenic $^{87}\text{Sr}/^{86}\text{Sr}$ isotope compositions observed in
123 Samoan shield lavas¹⁰ (red, Fig. 1), and are capped by late-stage volcanism with a characteristic
124 low $^{206}\text{Pb}/^{204}\text{Pb}$ and elevated $^{87}\text{Sr}/^{86}\text{Sr}$ isotope composition^{44,46} (green, Fig. 1, Extended Data Fig.
125 3). Magellan seamount compositions and ages⁴ are reassessed here, revealing a Samoan shield to
126 rejuvenated stage isotopic sequence⁴⁶ at Hemler and Vlinder Seamounts, while samples obtained
127 from the younger Magellan Seamounts are similar to Samoan late stage rejuvenated compositions
128 (Extended Data Fig. 3).

129 APM models for the predicted tracks of the high $^{206}\text{Pb}/^{204}\text{Pb}$ Rurutu-Arago hotspot and the
130 high $^{87}\text{Sr}/^{86}\text{Sr}$ Samoa hotspot suggest these two hotspot tracks should continue into the Mariana
131 Trench^{7,47} (Fig. 1). Geochemical data on Mariana arc volcanoes provides further support that the
132 Rurutu-Arago and Samoa hotspot tracks are subducted near the region proposed by APM models.
133 When the isotopic compositions of the Mariana arc volcanoes are examined, an unusual
134 geographically constrained high $^{206}\text{Pb}/^{204}\text{Pb}$ anomaly⁴⁵⁻⁴⁸ and an adjacent high $^{87}\text{Sr}/^{86}\text{Sr}$ anomaly
135 (which overlaps, but is shifted slightly to the south) are found where the Rurutu-Arago and Samoa
136 hotspot tracks are predicted to subduct based on the revised APM model (Fig. 1, Extended Data
137 Fig. 4). Consistent with the hypothesis that the subduction of seamounts impacts the chemistry of
138 nearby arc volcanoes, the $^{206}\text{Pb}/^{204}\text{Pb}$ and $^{87}\text{Sr}/^{86}\text{Sr}$ anomalies in the Mariana arc provide
139 supporting evidence for the presence of the long-lived Rurutu-Arago and Samoan hotspot tracks

140 in the western Pacific during the Early Cretaceous. Furthermore, their offset position in the
141 Mariana arc also supports the presence of a more northerly Rurutu-Arago hotspot track in the
142 western Pacific region predicted by our new APM, which is different from predictions by prior
143 APM models (Fig. 1, Extended Data Fig. 4). Consequently, we now can explore Rurutu-Arago
144 and Samoa as a pair of long-lived parallel (but offset) hotspot tracks, providing a multi-hotspot
145 continuation of APM constraints beyond the 80 Ma limit that is provided by the Hawaii-Emperor
146 and Louisville hotspot tracks.

147 While the Rurutu-Arago hotspot track is defined by seamounts with related geochemical
148 fingerprints that closely follow APM models back to 80 Ma, existing APM models⁷ predict the
149 track to significantly bend to the west around the Wake Seamounts (Extended Data Fig. 4). This
150 region is only sparsely populated by seamounts when compared to the abundance of seamounts
151 around Wake Island and the Wake Seamounts, which provide a clearer morphological continuation
152 of the hotspot track as well as a geochemical and temporal match to the Rurutu-Arago hotspot^{29,47}
153 (Extended Data Fig. 4). The clear impact of Rurutu-Arago hotspot on Mariana arc
154 compositions^{47,48} (Extended Data Fig. 4) suggests that, in contrast to existing APM models, the
155 hotspot followed a more northerly track between 120 and 80 Ma—offset by >1200 km from
156 existing models. This alternative “northern path” (blue path in the Wake Seamounts in Fig. 1, “this
157 study” in Extended Data Fig. 4) for the pre-80 Ma Rurutu-Arago hotspot track provides a unified
158 explanation for all these observations – geochronological, geochemical, and geomorphological –
159 suggesting that a reconsideration of the APM models is warranted.

160 The period of plate motion covered by our new data is constrained by the ~80-100 Ma
161 Marshall Island volcanoes and Wake Island area seamounts. Critically, new and existing ⁴⁰Ar/³⁹Ar
162 ages for the two volcanic chains correspond with the 80-100 Ma single plate rotation (stage) of the
163 existing K01 plate motion model¹⁸. For the period prior to 80 Ma, modern APM models⁴⁹ still
164 define motion with the large time-step plate rotations of early models^{2,18}. Given the limited
165 availability of samples suitable for age determinations around Wake Island, we resort to a similar
166 approach as used in the K01 model³ and calculate plate motion using large time-steps rather than
167 applying a more continuous age model such as WK08³⁹. For the 80-100 Ma time interval, we
168 modeled the plate motion by finding the stage pole (0.7°S, 315.7°E) that minimizes the difference
169 in Euler pole distance between the actual seamounts and the predicted age progressive paths for

170 the Samoa and Rurutu-Arago hotspot tracks (Methods). Using the new modified APM model,
171 called K01m, our results show that the predicted track projects Rurutu-Arago through the Wake
172 area seamounts (blue path in Fig. 1), whereas prior models failed to reconstruct the positions of
173 the ~80-100 Ma Wake Islands and seamounts (Extended Data Fig. 4). Due to the southeasterly
174 shift in location of the K01m rotation pole compared to K01, the relative angular distances from
175 the Euler pole to Samoa and Rurutu-Arago have changed in a manner where the resulting predicted
176 path length for Samoa remains similar to older models, while that of Rurutu-Arago lengthens
177 significantly.

178 The application of this new 80-100 Ma rotation pole to the Louisville hotspot has profound
179 implications for linking the Louisville track to OJP-Nui. While prior plate motion models placed
180 the Louisville hotspot far from OJP at the time of eruption¹, the new 80-100 Ma rotation increases
181 the north-south component of the predicted Louisville path (Fig. 3). As a result, the new K01m
182 model using long-lived intraplate hotspots traces the predicted Louisville hotspot track directly
183 into the center of OJP-Nui by ~120 Ma, the modeled age of formation for the superplateau^{21,50}.
184 This is in contrast to existing APM models^{3,6,7,49} that all predict a more southerly track (Fig. 3) that
185 falls short of the OJP, most likely because these models incorporate near-ridge large structures
186 (rises) and seamounts in their datasets. An assessment of the fit of individual track segments using
187 backtracking with different APM models confirms this result (Methods; Extended Data Fig. 5).
188 The formation age of OJP-Nui has been estimated based on decades old lower quality ⁴⁰Ar/³⁹Ar
189 ages and plate reconstructions to be older than 120 Ma^{21,50}, yet recent high-precision
190 geochronology suggests that the main phase of OJP volcanism began around 116 Ma⁵¹. This makes
191 the reconstructed link between Louisville and OJP-Nui even more likely.

192 During the formation of the Louisville hotspot track from OJP-Nui until present day (Fig.
193 3), there remains two time periods with poor constraints. First, the 80-90 Ma Louisville Seamounts
194 all have subducted into the Tonga Trench, interrupting the direct connection between the OJP and
195 the Louisville seamount track. Second, the location of the earliest portion of the Louisville
196 seamount track between 90-116 Ma depends on whether or not the Manihiki or Hikurangi Plates
197 (and their associated plateaus) rotated during the break-up¹ of OJP-Nui (Fig. 3), and whether there
198 exists an eruptive age progression throughout OJP-Nui given that Manihiki may predate OJP by
199 up to 6 Ma⁵¹. In either case, the eruptive location of the earliest Louisville track is within the

200 OJP outline and, importantly, we show for the first time that 90-115 Ma seamounts in the Ellice
201 Basin agree with the expected age progression, location, and isotopic signature of Louisville
202 hotspot-related volcanoes in the region¹⁴ (Fig. 2). These seamounts therefore provide the “missing
203 link” connecting the OJP to the start of the Louisville track. The Louisville Seamounts and Ellice
204 Basin seamounts are geochemically similar and plot along the array defined by Manihiki’s Danger
205 Islands and OJP melts (Fig. 2; Methods). Therefore, the Louisville and Ellice Basin seamounts are
206 geochemically and temporally linked to OJP-Nui.

207 Our demonstrated fit of OJP-Nui to the Louisville hotspot track (Fig. 3; Extended Data Fig.
208 5) requires no significant plume motion, which agrees with estimates of limited latitudinal motion
209 of this hotspot between ~70-0 Ma⁸. Our new data, and new interpretation of existing data, thus
210 present a simple argument for the genetic connection between Louisville and OJP-Nui. This
211 implies a plume-driven origin for the largest LIP in the geologic record, in contrast to recent
212 arguments for a major role for seafloor spreading in the construction of LIPs, such as Shatsky
213 Rise³⁵. Renewed consideration for other Cretaceous “orphan” LIPs—that may still lack obvious
214 volcanic trails—is warranted, in light of the suggested revision to the 80-100 Ma stage pole that
215 may serve to further address identified uncertainties in Pacific APM during the Cretaceous.

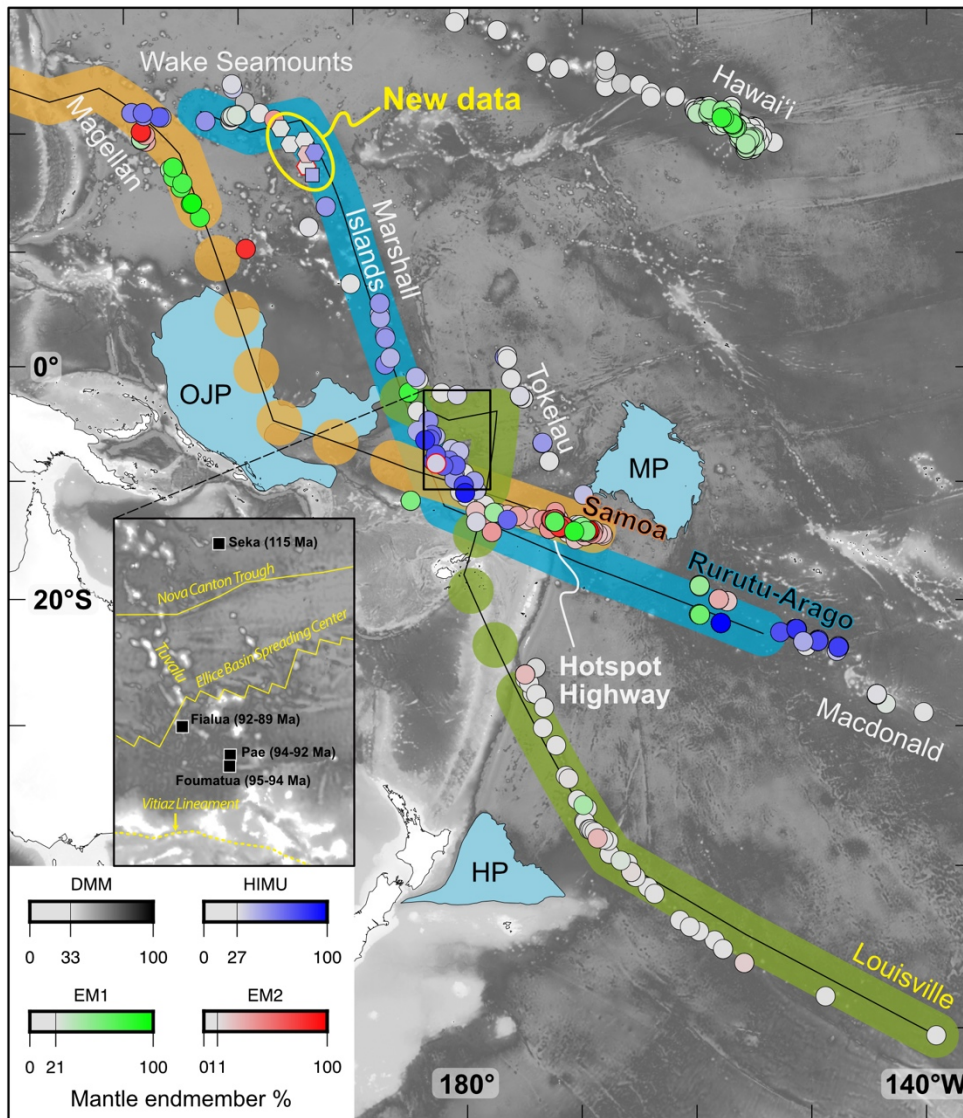
216 ACKNOWLEDGEMENTS

217 This work was supported by NOAA OER and GFOE, and is part of NSF-OCE project 1912934 to
218 JK and PW. AA was supported by NSF-REU grant 1560196 to PW. MJ was supported by NSF-
219 OCE project 1912931. AK was supported by NSF-OCE 1912932. We thank the crew and the team
220 of ROV pilots and engineers aboard the E/V *Okeanos Explorer* during the EX1606 expedition.
221 We thank John VanDecar for handling the editorial process and comments from two anonymous
222 reviewers that improved the manuscript. This manuscript is dedicated to the memories of our first
223 author, Jasper G. Konter and our co-author, Paul Wessel.

224

225 FIGURES

226



227

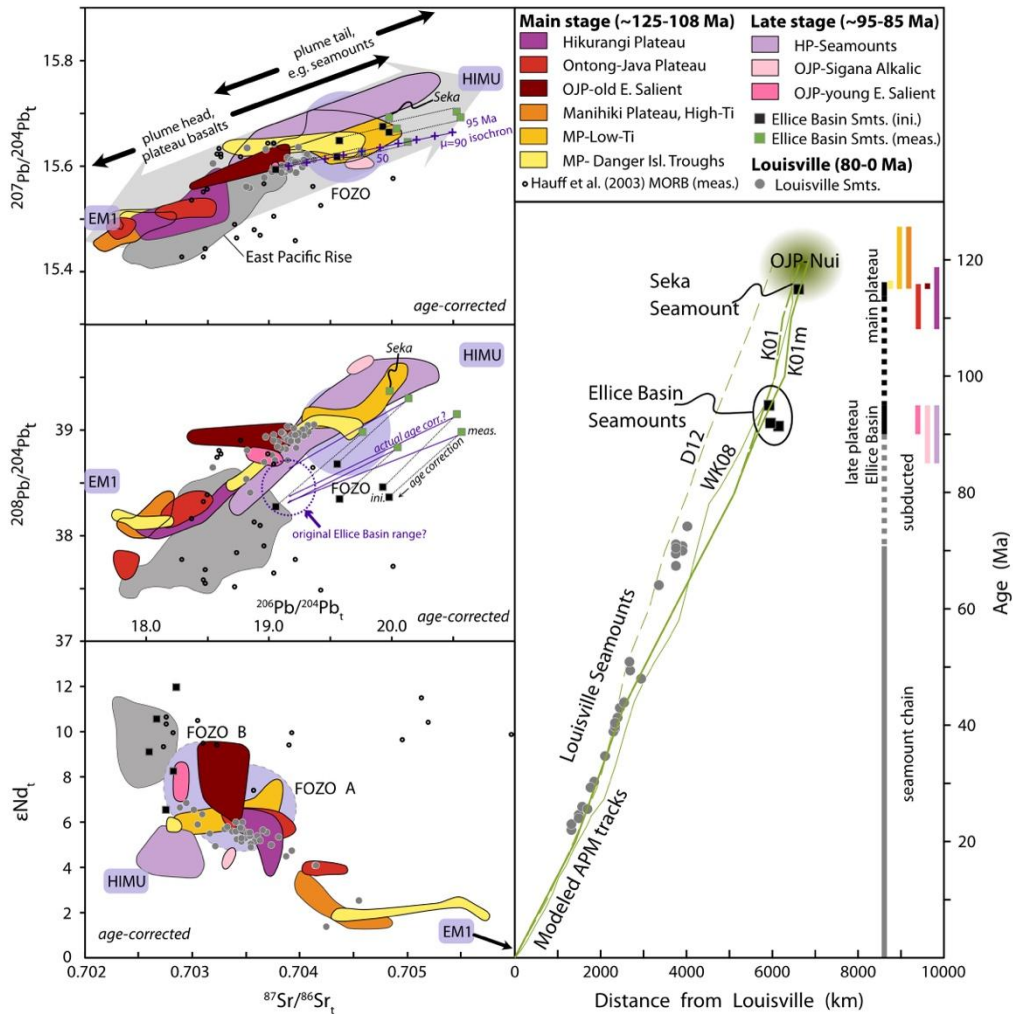
228

229 **Figure 1.** Pacific hotspot tracks and color-coded geochemical lava flow compositions (bottom
230 right inset, Methods) demonstrate unique signatures for Rurutu-Arago (blue circles) and Samoa
231 (red and green) and thus allow for the effective geochemical tracing of these hotspots, when
232 combined with seamount ages. New Wake region samples linked to Rurutu-Arago are shown as
233 hexagons; a Wake sample unrelated to Rurutu-Arago (see Methods) is shown with a square

234 *symbol. Ellice Basin Group and the New Wake samples with a red outline are confirmed*
235 *phosphatized (See Alteration section in Methods) and not considered in discussions of $^{143}\text{Nd}/^{144}\text{Nd}$*
236 *behavior. The colored tracks show predicted hotspot tracks following the new K01m APM*
237 *(specifically, 80-100 Ma stage represented by the Wake-Marshall and Magellan areas). The*
238 *dashed portions of the predicted Louisville hotspot track mark where the track was subducted. For*
239 *Louisville (green), the updated APM predicts an origin at Ontong-Java Plateau (OJP). The new*
240 *APM modeling relies on Wake-Marshall and Magellan seamounts, omitting the Shatsky and Mid-*
241 *Pac groups, and for the first time directly relates the Louisville hotspot to OJP. Hawaiian-Emperor*
242 *hotspot sample data are shown for reference. See the Supplementary Information for data sources.*
243 ***Inset:*** *Locations and ages of all Ellice Basin Seamounts and Seka Seamount, as confirmed by*
244 *geochronology, as black squares. The Tuvalu chain, Nova Canton Trough, Ellice Basin Spreading*
245 *Center, and Vitiaz Lineament are shown in yellow.*

246

247



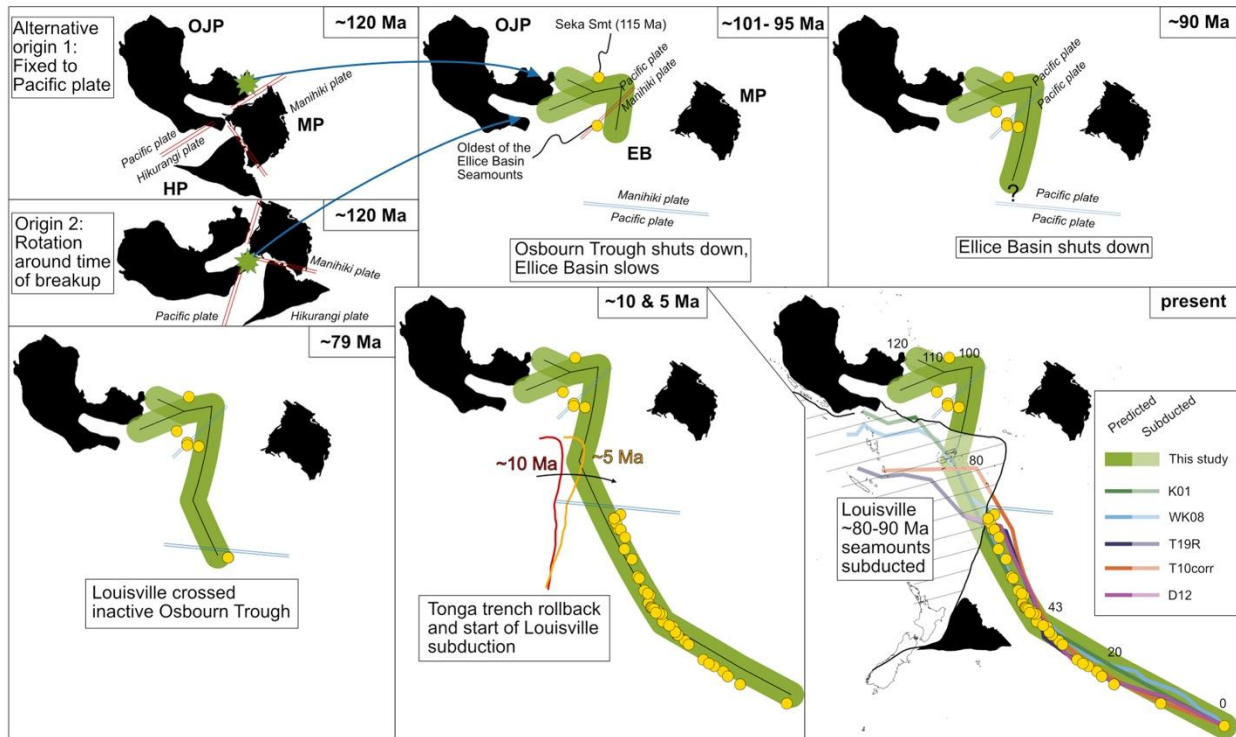
248

249 **Figure 2.** Right: Age progression for the Louisville hotspot track (symbols same as in plots). Ellice
 250 Basin Seamounts¹⁴ and Seka Seamount⁴⁴ are shown. Top: Age-corrected $^{207}\text{Pb}/^{204}\text{Pb}$ vs.
 251 $^{206}\text{Pb}/^{204}\text{Pb}$ isotope compositions for Ontong Java Nui, and related structures. Middle: Age-
 252 corrected $^{208}\text{Pb}/^{204}\text{Pb}$ vs. $^{206}\text{Pb}/^{204}\text{Pb}$ isotope compositions for Ontong Java Nui, and related
 253 structures. Bottom: $\varepsilon^{143}\text{Nd}_t$ vs. age-corrected $^{87}\text{Sr}/^{86}\text{Sr}$ for Ontong-Java Nui and related structures.
 254 Pb-isotope data for Ontong-Java (OJP), Manihiki (MP), and Hikurangi plateaus (HP), which
 255 represent the main pulses of voluminous plateau-building volcanism (~120 and ~90 Ma), are
 256 frequently less radiogenic, but extend to radiogenic values in some settings. By contrast, smaller
 257 structures such as seamounts are confined to intermediate-to-radiogenic values. Louisville and
 258 Ellice Basin seamounts exhibit more radiogenic Pb-isotopes, with Ellice Basin being particularly
 259 radiogenic due to seawater U influence, but likely a mixture of FOZO and DMM that originally

260 *resembled slightly depleted Louisville-type compositions (see Methods). Green squares are*
261 *present-day Ellice Basin compositions, compared to corresponding age-corrected (where*
262 *possible) compositions. Louisville seamounts overlap directly with some OJP basalts in Pb-Nd-Sr*
263 *isotope space, and are well within the array of compositions found in the greater combined set of*
264 *plateaus and structures from OJP, MP and HP. Furthermore, Ellice Basin and Seka seamounts*
265 *are spatiotemporally linked to the OJP. See Methods for description of isotopic data compared to*
266 *variations in plume head and plume tail stages of volcanic activity, analysis of Pb-Sr-Nd isotopic*
267 *systematics in the Ellice Basin Samples, and data sources.*

268

269



270

271 **Figure 3.** Cartoon of Louisville hotspot (green swath) evolution. The revised model predicts that
 272 the Louisville hotspot initiated within Ontong Java Plateau (OJP), however the exact initial
 273 location is sensitive to whether the plateaus rotated around the time of OJP-Nui breakup⁵⁰, so two
 274 alternatives are shown for ~120 Ma. By ~95 Ma, the Ellice Basin (EB) had (mostly) opened
 275 between OJP and Manihiki Plateau (MP), as suggested by the age of the oldest Ellice Basin
 276 Seamounts (95.0 Ma¹⁴)—located centrally in the basin—which we link to the Louisville hotspot.
 277 Seka Seamount (115.0 Ma⁴⁴), located at the north end of the basin, is isotopically similar to the
 278 Ellice Basin seamounts (suggesting significant Ellice Basin spreading occurred by 115 Ma) and
 279 is also linked to the Louisville hotspot. The new model predicts Louisville to be present in the Ellice
 280 Basin at this time, progressing to younger ages to the south. The oldest Louisville Seamount
 281 erupted at ~79 Ma^{8,36}, located south of the Osbourn Trough, represents the oldest part of the
 282 continuously defined Louisville hotspot track. In the past 5 to 10 Ma, roll-back of the Tonga Trench
 283 caused the subduction of any Louisville Seamounts with ages between 79 to 90 Ma, leaving only
 284 the older (>90 Ma) Louisville hotspot-related structures in the Ellice Basin and OJP areas
 285 preserved. Consequently, the relationship between >79 Ma Louisville hotspot volcanism and the

This is a preprint of an article that has been submitted to Nature, and revised based on two rounds of peer review, but has yet to be formally accepted for publication.

286 *paleoridge represented by the Osbourn Trough is unclear. Predicted hotspot tracks show that only*
287 *the new model tracks Louisville hotspot back to OJP-Nui, specifically the OJP. See Methods for*
288 *details on this model.*

289

290 **REFERENCES**

- 291 1. Chandler, M. T., Wessel, P. & Sager, W. W. Analysis of Ontong Java Plateau
292 palaeolatitudes: evidence for large-scale rotation since 123 Ma? *Geophys. J. Int.* **194**, 18–29
293 (2013).
- 294 2. Duncan, R. A. & Clague, D. A. Pacific Plate Motion Recorded by Linear Volcanic Chains. in
295 *The Ocean Basins and Margins: Volume 7A The Pacific Ocean* (eds. Nairn, A. E. M., Stehli,
296 F. G. & Uyeda, S.) 89–121 (Springer US, Boston, MA, 1985). doi:10.1007/978-1-4613-
297 2351-8_3.
- 298 3. Koppers, A. A. P. *et al.* Mantle plumes and their role in Earth processes. *Nat. Rev. Earth*
299 *Environ.* **2**, 382–401 (2021).
- 300 4. Koppers, A. A. P. & Sager, W. W. Chapter 4.3 - Large-Scale and Long-Term Volcanism on
301 Oceanic Lithosphere. in *Developments in Marine Geology* (eds. Stein, R., Blackman, D. K.,
302 Inagaki, F. & Larsen, H.-C.) vol. 7 553–597 (Elsevier, 2014).
- 303 5. Tarduno, J., Bunge, H.-P., Sleep, N. & Hansen, U. The Bent Hawaiian-Emperor Hotspot
304 Track: Inheriting the Mantle Wind. *Science* **324**, 50–53 (2009).
- 305 6. Doubrovine, P. V., Steinberger, B. & Torsvik, T. H. Absolute plate motions in a reference
306 frame defined by moving hot spots in the Pacific, Atlantic, and Indian oceans. *J. Geophys.*
307 *Res. Solid Earth* **117**, (2012).
- 308 7. Wessel, P. & Kroenke, L. W. Observations of geometry and ages constrain relative motion of
309 Hawaii and Louisville plumes. *Earth Planet. Sci. Lett.* **284**, 467–472 (2009).
- 310 8. Koppers, A. A. P., Staudigel, H., Phipps Morgan, J. & Duncan, R. A. Nonlinear ⁴⁰Ar/³⁹Ar
311 age systematics along the Gilbert Ridge and Tokelau Seamount Trail and the timing of the
312 Hawaii-Emperor Bend. *Geochem. Geophys. Geosystems* **8**, n/a-n/a (2007).

- 313 9. Konrad, K. *et al.* On the relative motions of long-lived Pacific mantle plumes. *Nat. Commun.*
314 **9**, 854 (2018).
- 315 10. Jackson, M. G. *et al.* Helium and lead isotopes reveal the geochemical geometry of the
316 Samoan plume. *Nature* **514**, 355–358 (2014).
- 317 11. Jackson, M. G. *et al.* Samoan hot spot track on a “hot spot highway”: Implications for mantle
318 plumes and a deep Samoan mantle source. *Geochem. Geophys. Geosystems* **11**, n/a-n/a
319 (2010).
- 320 12. Konter, J. G. & Jackson, M. G. Large volumes of rejuvenated volcanism in Samoa: Evidence
321 supporting a tectonic influence on late-stage volcanism. *Geochem. Geophys. Geosystems* **13**,
322 n/a-n/a (2012).
- 323 13. Koppers, A. A. P. *et al.* Limited latitudinal mantle plume motion for the Louisville hotspot.
324 *Nat. Geosci.* **5**, 911–917 (2012).
- 325 14. Finlayson, V. A. *et al.* Sr–Pb–Nd–Hf isotopes and $^{40}\text{Ar}/^{39}\text{Ar}$ ages reveal a Hawaii–
326 Emperor-style bend in the Rurutu hotspot. *Earth Planet. Sci. Lett.* **500**, 168–179 (2018).
- 327 15. Richards, M. A., Duncan, R. A. & Courtillot, V. E. Flood Basalts and Hot-Spot Tracks:
328 Plume Heads and Tails. *Science* **246**, 103–107 (1989).
- 329 16. Courtillot, V., Davaille, A., Besse, J. & Stock, J. Three distinct types of hotspots in the
330 Earth’s mantle. *Earth Planet. Sci. Lett.* **205**, 295–308 (2003).
- 331 17. Konter, J. G. & Becker, T. W. Shallow lithospheric contribution to mantle plumes revealed
332 by integrating seismic and geochemical data. *Geochem. Geophys. Geosystems* **13**, n/a-n/a
333 (2012).

- 334 18. Koppers, A. A. P., Morgan, J. P., Morgan, J. W. & Staudigel, H. Testing the fixed hotspot
335 hypothesis using $40\text{Ar}/39\text{Ar}$ age progressions along seamount trails. *Earth Planet. Sci. Lett.*
336 16 (2001).
- 337 19. Campbell, I. H., Griffiths, R. W. & Hill, R. I. Melting in an Archaean mantle plume: heads
338 it's basalts, tails it's komatiites. *Nature* **339**, 697–699 (1989).
- 339 20. Coffin, Millard F. & Eldholm, Olav. Large igneous provinces: Crustal structure, dimensions,
340 and external consequences. *Rev. Geophys.* **32**, 1–36 (1994).
- 341 21. Taylor, B. The single largest oceanic plateau: Ontong Java–Manihiki–Hikurangi. *Earth*
342 *Planet. Sci. Lett.* **241**, 372–380 (2006).
- 343 22. Mahoney, J. J. & Spencer, K. J. Isotopic evidence for the origin of the Manihiki and Ontong
344 Java oceanic plateaus. *Earth Planet. Sci. Lett.* **104**, 196–210 (1991).
- 345 23. Golowin, R. *et al.* Geochemistry of deep Manihiki Plateau crust: Implications for
346 compositional diversity of large igneous provinces in the Western Pacific and their genetic
347 link. *Chem. Geol.* **493**, 553–566 (2018).
- 348 24. Henderson, L. & Gordon, R. G. Oceanic plateaus and the motion of the Pacific plate with
349 respect to the hotspots. *Eos Trans. Am. Geophys. Union* **62**, 1028 (1981).
- 350 25. Antretter, M., Riisager, P., Hall, S., Zhao, X. & Steinberger, B. Modelled palaeolatitudes for
351 the Louisville hot spot and the Ontong Java Plateau. *Geol. Soc. Lond. Spec. Publ.* **229**, 21–30
352 (2004).
- 353 26. Kroenke, L. W., Wessel, P. & Sterling, A. Motion of the Ontong Java Plateau in the hot-spot
354 frame of reference: 122 Ma-present. *Geol. Soc. Lond. Spec. Publ.* **229**, 9–20 (2004).

- 355 27. Neal, C., Mahoney, J., Kroenke, L., Duncan, R. & Petterson, M. The Ontong Java Plateau.
356 *Wash. DC Am. Geophys. Union Geophys. Monogr. Ser.* 183–216 (1997)
357 doi:10.1029/GM100p0183.
- 358 28. Vanderkluysen, L. *et al.* Louisville Seamount Chain: Petrogenetic processes and
359 geochemical evolution of the mantle source. *Geochem. Geophys. Geosystems* **15**, 2380–2400
360 (2014).
- 361 29. Koppers, A. A. P., Staudigel, H., Pringle, M. S. & Wijbrans, J. R. Short-lived and
362 discontinuous intraplate volcanism in the South Pacific: Hot spots or extensional volcanism?
363 *Geochem. Geophys. Geosystems* **4**, n/a-n/a (2003).
- 364 30. Sager, W. W. *et al.* Oceanic plateau formation by seafloor spreading implied by Tamu
365 Massif magnetic anomalies. *Nat. Geosci.* **12**, 661–666 (2019).
- 366 31. Kopp, H. *et al.* Fossil hot spot-ridge interaction in the Musicians Seamount Province:
367 Geophysical investigations of hot spot volcanism at volcanic elongated ridges. *J. Geophys.*
368 *Res. Solid Earth* **108**, (2003).
- 369 32. O'Connor, J. M. *et al.* Deformation-related volcanism in the Pacific Ocean linked to the
370 Hawaiian–Emperor bend. *Nat. Geosci.* **8**, 393–397 (2015).
- 371 33. Fletcher, M., Wyman, D. A. & Zahirovic, S. Mantle plumes, triple junctions and transforms:
372 A reinterpretation of Pacific Cretaceous – Tertiary LIPs and the Laramide connection.
373 *Geosci. Front.* **11**, 1133–1144 (2020).
- 374 34. Davis, A. S., Gray, L. B., Clague, D. A. & Hein, J. R. The Line Islands revisited: New
375 ⁴⁰Ar/³⁹Ar geochronologic evidence for episodes of volcanism due to lithospheric extension.
376 *Geochem. Geophys. Geosystems* **3**, 1–28 (2002).
- 377 35. Sager, W. W. What built Shatsky Rise, a mantle plume or ridge tectonics? 15.

- 378 36. Heaton, D. E. & Koppers, A. a. P. High-Resolution $^{40}\text{Ar}/^{39}\text{Ar}$ Geochronology of the
379 Louisville Seamounts IODP Expedition 330 Drill Sites: Implications for the Duration of Hot
380 Spot-related Volcanism and Age Progressions. *Geochem. Geophys. Geosystems* **20**, 4073–
381 4102 (2019).
- 382 37. Bono, R. K., Tarduno, J. A. & Bunge, H.-P. Hotspot motion caused the Hawaiian-Emperor
383 Bend and LLSVPs are not fixed. *Nat. Commun.* **10**, 3370 (2019).
- 384 38. Cande, S. C., Raymond, C. A., Stock, J. & Haxby, W. F. Geophysics of the Pitman Fracture
385 Zone and Pacific-Antarctic Plate Motions During the Cenozoic. *Sci. New Ser.* **270**, 947–953
386 (1995).
- 387 39. Wessel, P. & Kroenke, L. W. Pacific absolute plate motion since 145 Ma: An assessment of
388 the fixed hot spot hypothesis. *J. Geophys. Res.* **113**, (2008).
- 389 40. O'Connor, J. M. *et al.* Constraints on past plate and mantle motion from new ages for the
390 Hawaiian-Emperor Seamount Chain: HAWAIIAN-EMPEROR SEAMOUNT CHAIN
391 AGES. *Geochem. Geophys. Geosystems* **14**, 4564–4584 (2013).
- 392 41. Staudigel, H., Koppers, A. A. P., Plank, T. A. & Hanan, B. B. Seamounts in the Subduction
393 Factory. *Oceanography* **23**, 176–181 (2010).
- 394 42. Janney, P. E. & Castillo, P. R. Isotope geochemistry of the Darwin Rise seamounts and the
395 nature of long-term mantle dynamics beneath the south central Pacific. *J. Geophys. Res.*
396 *Solid Earth* **104**, 10571–10589 (1999).
- 397 43. Jackson, M. G. *et al.* The return of subducted continental crust in Samoan lavas. *Nature* **448**,
398 684–687 (2007).
- 399 44. Konter, J. G. *et al.* One hundred million years of mantle geochemical history suggest the
400 retiring of mantle plumes is premature. *Earth Planet. Sci. Lett.* **275**, 285–295 (2008).

- 401 45. Price, A. A. *et al.* Distinguishing Volcanic Contributions to the Overlapping Samoan and
402 Cook-Austral Hotspot Tracks. *J. Petrol.* **63**, egac032 (2022).
- 403 46. Reinhard, A. A. *et al.* “Petit Spot” Rejuvenated Volcanism Superimposed on Plume-Derived
404 Samoan Shield Volcanoes: Evidence From a 645-m Drill Core From Tutuila Island,
405 American Samoa. *Geochem. Geophys. Geosystems* **20**, 1485–1507 (2019).
- 406 47. Staudigel, H. *et al.* The longevity of the South Pacific isotopic and thermal anomaly. *Earth*
407 *Planet. Sci. Lett.* **102**, 24–44 (1991).
- 408 48. Stern, R. J., Fouch, M. J. & Klemperer, S. L. An overview of the Izu-Bonin-Mariana
409 subduction factory. *Wash. DC Am. Geophys. Union Geophys. Monogr. Ser.* **138**, 175–222
410 (2003).
- 411 49. Torsvik, T. H. *et al.* Pacific-Panthalassic Reconstructions: Overview, Errata and the Way
412 Forward. *Geochem. Geophys. Geosystems* **20**, 3659–3689 (2019).
- 413 50. Chandler, M. T. *et al.* Reconstructing Ontong Java Nui: Implications for Pacific absolute
414 plate motion, hotspot drift and true polar wander. *Earth Planet. Sci. Lett.* **331–332**, 140–151
415 (2012).
- 416 51. Davidson, P. C., Koppers, A. A. P., Sano, T. & Hanyu, T. A younger and protracted
417 emplacement of the Ontong Java Plateau. *Science* **380**, 1185–1188 (2023).
- 418 52. Jochum, K. P. *et al.* GeoReM: A New Geochemical Database for Reference Materials and
419 Isotopic Standards. *Geostand. Geoanalytical Res.* **29**, 333–338 (2005).
- 420 53. Konter, J. G. & Storm, L. P. High precision $^{87}\text{Sr}/^{86}\text{Sr}$ measurements by MC-ICP-MS,
421 simultaneously solving for Kr interferences and mass-based fractionation. *Chem. Geol.* **385**,
422 26–34 (2014).

- 423 54. Todt, W., Cliff, R., Hanser, A. & Hofmann, A. Evaluation of a ^{202}Pb - ^{205}Pb double spike
424 for high - Precision lead isotope analysis. *Geophys. Monogr. Ser.* **95**, 429–437 (1996).
- 425 55. Abouchami, W., Galer, S. J. G. & Hofmann, A. W. High precision lead isotope systematics
426 of lavas from the Hawaiian Scientific Drilling Project. *Chem. Geol.* **169**, 187–209 (2000).
- 427 56. Münker, C., Weyer, S., Scherer, E. & Mezger, K. Separation of high field strength elements
428 (Nb, Ta, Zr, Hf) and Lu from rock samples for MC-ICPMS measurements: SEPARATION
429 OF HIGH FIELD STRENGTH ELEMENTS. *Geochem. Geophys. Geosystems* **2**, n/a-n/a
430 (2001).
- 431 57. Béguelin, P., Bizimis, M., Beier, C. & Turner, S. Rift–plume interaction reveals multiple
432 generations of recycled oceanic crust in Azores lavas. *Geochim. Cosmochim. Acta* **218**, 132–
433 152 (2017).
- 434 58. Blichert-Toft, J. & Albarède, F. The Lu-Hf isotope geochemistry of chondrites and the
435 evolution of the mantle-crust system. *Earth Planet. Sci. Lett.* **148**, 243–258 (1997).
- 436 59. Koppers, A. A. P. ArArCALC—software for $^{40}\text{Ar}/^{39}\text{Ar}$ age calculations. *Comput. Geosci.*
437 **28**, 605–619 (2002).
- 438 60. Min, K., Mundil, R., Renne, P. R. & Ludwig, K. R. A test for systematic errors in $^{40}\text{Ar}/^{39}\text{Ar}$
439 geochronology through comparison with U/Pb analysis of a 1.1-Ga rhyolite. *Geochim.*
440 *Cosmochim. Acta* **64**, 73–98 (2000).
- 441 61. Kuiper, K. F. *et al.* Synchronizing Rock Clocks of Earth History. *Science* **320**, 500–504
442 (2008).
- 443 62. Lee, J.-Y. *et al.* A redetermination of the isotopic abundances of atmospheric Ar. *Geochim.*
444 *Cosmochim. Acta* **70**, 4507–4512 (2006).

- 445 63. Schaen, A. J. *et al.* Interpreting and reporting $^{40}\text{Ar}/^{39}\text{Ar}$ geochronologic data. *GSA Bull.*
446 **133**, 461–487 (2021).
- 447 64. Allègre, C. J., Hamelin, B., Provost, A. & Dupré, B. Topology in isotopic multispace and
448 origin of mantle chemical heterogeneities. *Earth Planet. Sci. Lett.* **81**, 319–337 (1987).
- 449 65. Hart, S. R. *et al.* Genesis of the Western Samoa seamount province: age, geochemical
450 fingerprint and tectonics. *Earth Planet. Sci. Lett.* **227**, 37–56 (2004).
- 451 66. Zindler, A. & Hart, Stan. *Chemical Geodynamics*. 79 (1986).
- 452 67. Hanan, B. B. & Graham, D. W. Lead and Helium Isotope Evidence from Oceanic Basalts for
453 a Common Deep Source of Mantle Plumes. *Sci. New Ser.* **272**, 991–995 (1996).
- 454 68. Smith, W. H. F., Staudigel, H., Watts, A. B. & Pringle, M. S. The Magellan seamounts:
455 Early Cretaceous record of the South Pacific isotopic and thermal anomaly. *J. Geophys. Res.*
456 *Solid Earth* **94**, 10501–10523 (1989).
- 457 69. Morgan, W. Jason. Deep Mantle Convection Plumes and Plate Motions. *AAPG Bull.* **56**,
458 (1972).
- 459 70. Steinberger, B., Sutherland, R. & O’Connell, R. J. Prediction of Emperor-Hawaii seamount
460 locations from a revised model of global plate motion and mantle flow. *Nature* **430**, 167–173
461 (2004).
- 462 71. Duncan, R. A. & Keller, R. A. Radiometric ages for basement rocks from the Emperor
463 Seamounts, ODP Leg 197. *Geochem. Geophys. Geosystems* **5**, (2004).
- 464 72. Koppers, A. A. P., Duncan, R. A. & Steinberger, B. Implications of a nonlinear $^{40}\text{Ar}/^{39}\text{Ar}$
465 age progression along the Louisville seamount trail for models of fixed and moving hot
466 spots. *Geochem. Geophys. Geosystems* **5**, (2004).

- 467 73. Seton, M. *et al.* Global continental and ocean basin reconstructions since 200Ma. *Earth-Sci.*
468 *Rev.* **113**, 212–270 (2012).
- 469 74. Hochmuth, K., Gohl, K. & Uenzelmann-Neben, G. Playing jigsaw with Large Igneous
470 Provinces-A plate tectonic reconstruction of Ontong Java Nui, West Pacific. *Geochem.*
471 *Geophys. Geosystems* **16**, 3789–3807 (2015).
- 472 75. Zhang, G.-L. & Li, C. Interactions of the Greater Ontong Java mantle plume component with
473 the Osbourn Trough. *Sci. Rep.* **6**, 37561 (2016).
- 474 76. Wobbe, F., Gohl, K., Chambord, A. & Sutherland, R. Structure and breakup history of the
475 rifted margin of West Antarctica in relation to Cretaceous separation from Zealandia and
476 Bellingshausen plate motion. *Geochem. Geophys. Geosystems* **13**, (2012).
- 477 77. Mortimer, N. *et al.* Late Cretaceous oceanic plate reorganization and the breakup of
478 Zealandia and Gondwana. *Gondwana Res.* **65**, 31–42 (2019).
- 479 78. Benyshek, E. K., Wessel, P. & Taylor, B. Tectonic Reconstruction of the Ellice Basin.
480 *Tectonics* **38**, 3854–3865 (2019).
- 481 79. Konter, J. G. *et al.* Geochemical stages at Jasper Seamount and the origin of intraplate
482 volcanoes. *Geochem. Geophys. Geosystems* **10**, n/a-n/a (2009).
- 483 80. Koppers, A. A. P. Asynchronous Bends in Pacific Seamount Trails: A Case for Extensional
484 Volcanism? *Science* **307**, 904–907 (2005).
- 485 81. Hart, S. R., Hauri, E. H., Oschmann, L. A. & Whitehead, J. A. Mantle Plumes and
486 Entrainment: Isotopic Evidence. *Science* **256**, 517–520 (1992).
- 487 82. Koppers, A. A. P. *et al.* Samoa reinstated as a primary hotspot trail. *Geology* **36**, 435 (2008).

- 488 83. Koppers, A. A. P., Staudigel, H., Wijbrans, J. R. & Pringle, M. S. The Magellan seamount
489 trail: implications for Cretaceous hotspot volcanism and absolute Pacific plate motion. *Earth*
490 *Planet. Sci. Lett.* **163**, 53–68 (1998).
- 491 84. Koppers, A. A. P. *et al.* New ⁴⁰Ar/³⁹Ar age progression for the Louisville hot spot trail and
492 implications for inter-hot spot motion. *Geochem. Geophys. Geosystems* **12**, n/a-n/a (2011).
- 493 85. Koppers, A. A. P. *et al.* Age systematics of two young en echelon Samoan volcanic trails.
494 *Geochem. Geophys. Geosystems* **12**, n/a-n/a (2011).
- 495 86. Coffin, M. F. *et al.* Large igneous provinces and scientific ocean drilling: status quo and a
496 look ahead. *Oceanography* **19**, 150–160 (2006).
- 497 87. Harrison, L. N. & Weis, D. The Size and Emergence of Geochemical Heterogeneities in the
498 Hawaiian Mantle Plume Constrained by Sr-Nd-Hf Isotopic Variation Over ~47 Million
499 Years. *Geochem. Geophys. Geosystems* **19**, 2823–2842 (2018).
- 500 88. Harrison, L. N., Weis, D. & Garcia, M. O. The link between Hawaiian mantle plume
501 composition, magmatic flux, and deep mantle geodynamics. *Earth Planet. Sci. Lett.* **463**,
502 298–309 (2017).
- 503 89. Harrison, L. N., Weis, D. & Garcia, M. O. The multiple depleted mantle components in the
504 Hawaiian-Emperor chain. *Chem. Geol.* **532**, 119324 (2020).
- 505 90. Wei, X. *et al.* Co-Occurrence of HIMU and EM1 Components in a Single Magellan
506 Seamount: Implications for the Formation of West Pacific Seamount Province. *J. Petrol.* **63**,
507 egac022 (2022).
- 508 91. Bonneville, A., Dosso, L. & Hildenbrand, A. Temporal evolution and geochemical
509 variability of the South Pacific superplume activity. *Earth Planet. Sci. Lett.* **244**, 251–269
510 (2006).

- 511 92. Buff, L. *et al.* “Missing links” for the long-lived Macdonald and Arago hotspots, South
512 Pacific Ocean. *Geology* **49**, 541–544 (2021).
- 513 93. Class, C. & Lehnert, K. PetDB expert MORB (mid-ocean ridge basalt) compilation. (2012).
- 514 94. Mahoney, J. J., Storey, M., Duncan, R. A., Spencer, K. J. & Pringle, M. Geochemistry and
515 age of the Ontong Java Plateau. *Wash. DC Am. Geophys. Union Geophys. Monogr. Ser.* **77**,
516 233–261 (1993).
- 517 95. Tejada, M. L. G., Mahoney, J. J., Duncan, R. A. & Hawkins, M. P. Age and Geochemistry of
518 Basement and Alkalic Rocks of Malaita and Santa Isabel, Solomon Islands, Southern Margin
519 of Ontong Java Plateau. *J. Petrol.* **37**, 361–394 (1996).
- 520 96. Tejada, M. L. G. *et al.* Pin-pricking the elephant: evidence on the origin of the Ontong Java
521 Plateau from Pb-Sr-Hf-Nd isotopic characteristics of ODP Leg 192 basalts. *Geol. Soc. Lond.*
522 *Spec. Publ.* **229**, 133–150 (2004).
- 523 97. Tejada, M. L. G. Basement Geochemistry and Geochronology of Central Malaita, Solomon
524 Islands, with Implications for the Origin and Evolution of the Ontong Java Plateau. *J. Petrol.*
525 **43**, 449–484 (2002).
- 526 98. Hoernle, K. *et al.* Age and geochemistry of volcanic rocks from the Hikurangi and Manihiki
527 oceanic Plateaus. *Geochim. Cosmochim. Acta* **74**, 7196–7219 (2010).
- 528 99. Timm, C. *et al.* Age and geochemistry of the oceanic Manihiki Plateau, SW Pacific: New
529 evidence for a plume origin. *Earth Planet. Sci. Lett.* **304**, 135–146 (2011).
- 530 100. Ingle, S. *et al.* Depleted mantle wedge and sediment fingerprint in unusual basalts from
531 the Manihiki Plateau, central Pacific Ocean. *Geology* **35**, 595 (2007).
- 532 101. Hauff, F., Hoernle, K. & Schmidt, A. Sr-Nd-Pb composition of Mesozoic Pacific oceanic
533 crust (Site 1149 and 801, ODP Leg 185): Implications for alteration of ocean crust and the

- 534 input into the Izu-Bonin-Mariana subduction system. *Geochem. Geophys. Geosystems* **4**,
535 (2003).
- 536 102. Geldmacher, J. *et al.* The effects of submarine alteration and phosphatization on igneous
537 rocks: Implications for Sr-, Nd-, Pb-isotope studies. *Chem. Geol.* **631**, 121509 (2023).
- 538 103. Beier, C., Vanderkluysen, L., Regelous, M., Mahoney, J. J. & Garbe-Schönberg, D.
539 Lithospheric control on geochemical composition along the Louisville Seamount Chain.
540 *Geochem. Geophys. Geosystems* **12**, n/a-n/a (2011).
- 541 104. Kingsley, R. H., Blichert-Toft, J., Fontignie, D. & Schilling, J.-G. Hafnium, neodymium,
542 and strontium isotope and parent-daughter element systematics in basalts from the plume-
543 ridge interaction system of the Salas y Gomez Seamount Chain and Easter Microplate.
544 *Geochem. Geophys. Geosystems* **8**, n/a-n/a (2007).
- 545 105. Regelous, M. Geochemistry of Lavas from the Emperor Seamounts, and the Geochemical
546 Evolution of Hawaiian Magmatism from 85 to 42 Ma. *J. Petrol.* **44**, 113–140 (2003).
- 547 106. Nebel, O. *et al.* Coupled Hf–Nd–Pb isotope co-variations of HIMU oceanic island basalts
548 from Mangaia, Cook-Austral islands, suggest an Archean source component in the mantle
549 transition zone. *Geochim. Cosmochim. Acta* **112**, 87–101 (2013).
- 550 107. Sun, S. -s. & McDonough, W. F. Chemical and isotopic systematics of oceanic basalts:
551 implications for mantle composition and processes. *Geol. Soc. Lond. Spec. Publ.* **42**, 313–
552 345 (1989).
- 553 108. Hart, S. R. & Blusztajn, J. Age and geochemistry of the mafic sills, ODP site 1276,
554 Newfoundland margin. *Chem. Geol.* **235**, 222–237 (2006).

- 555 109. Ruellan, E., Delteil, J., Wright, I. & Matsumoto, T. From rifting to active spreading in the
556 Lau Basin – Havre Trough backarc system (SW Pacific): Locking/unlocking induced by
557 seamount chain subduction. *Geochem. Geophys. Geosystems* **4**, (2003).
- 558 110. Torsvik, T. H., Steinberger, B., Gurnis, M. & Gaina, C. Plate tectonics and net
559 lithosphere rotation over the past 150My. *Earth Planet. Sci. Lett.* **291**, 106–112 (2010).
- 560 111. Müller, R. D. *et al.* A Global Plate Model Including Lithospheric Deformation Along
561 Major Rifts and Orogens Since the Triassic. *Tectonics* **38**, 1884–1907 (2019).
- 562 112. Regelous, M. *et al.* Mantle dynamics and mantle melting beneath Niufo’ou Island and
563 the northern Lau back-arc basin. *Contrib. Mineral. Petrol.* **156**, 103–118 (2008).
- 564 113. Tarduno, J. A. *et al.* The Emperor Seamounts: Southward Motion of the Hawaiian
565 Hotspot Plume in Earth’s Mantle. *Sci. New Ser.* **301**, 1064–1069 (2003).

566

567

568

569

570 **METHODS**

571 **Sample analysis for mantle source composition**

572 Samples were collected with ROV *Deep Discoverer*, aboard the NOAA exploration vessel
573 *Okeanos Explorer*, during expedition EX1606 to the Wake Island Unit of the U.S. Pacific
574 Remote Island Marine National Monument. Dive samples were cut open and the seven least
575 altered samples were selected. All compositional data for the new Wake samples are found in
576 Supplementary Data Table 1.

577 Major elements collected by laser induced breakdown spectroscopy, using a Nd-YAG 20 mJ
578 pulsed laser and a Catalina Scientific EMU-120 echelle spectrometer. Major element
579 compositions were calibrated against 36 different standards, using partial least squares (PLS)
580 regression, in MATLAB. Predicted compositions of unknown samples using PLS show typically
581 <2 wt.% variability on repeat analyses, after each sample is re-normalized to 100% total values.

582 Trace element data were obtained using a ThermoFinnegan Element2 ICP-MS (University of
583 South Carolina). Aliquots of sample powders were lightly leached with 0.1N HCl in a sonic bath
584 for 20 minutes to mitigate any low-temperature overprinting by seawater without compromising
585 the primary bulk composition. The sample powders were then dissolved in Teflon-distilled
586 HF:HNO₃ mixture, subsequently dissolved in 2 wt.% HNO₃, and spiked with In at 2 ppb
587 concentration in the solution. The USGS reference material BHVO-2 was used as a standard and
588 the reference materials BCR-2 and JB-2 were run as unknowns along the samples. The
589 calculated concentrations for the unknowns agree well within 5% for most elements relative to
590 the recommended concentrations from GEOREM (accessed, August 2022⁵²).

591 Pb-Sr-Nd-Hf isotopic compositions were obtained following mechanical and chemical
592 procedures to remove seafloor alteration contributions⁴ and previously detailed elemental
593 separation procedures⁵³. In short, a small piece from the center of each sample was crushed,
594 altered pieces were removed by hand-picking, the ~500-1000 μm clean fraction was acid-leached
595 in several steps, all done on a hot plate at ~80-100 C: ~1 hour each in 2M HNO₃, 6N HCl, and
596 4M HNO₃, before undergoing a final ~16 hour leach in 6N HCl. Samples were subsequently
597 dissolved for sequential recovery of Sr, Pb, Nd, and Hf. An aliquot of unleached BCR-2 powder

598 was digested alongside the samples as a quality monitor and is reported in Supplemental Data
599 Table 2. Pb was separated and purified with Sr-Spec resin and AG1-x8 resin, respectively⁵³.
600 Isotope measurements were performed on a Nu Plasma HR MC-ICP-MS at the University of
601 Hawai'i at Mānoa (Pb, except for EX1606-D3-3) using sample standard bracketing, and Tl
602 doping to monitor fractionation. Repeatability of Pb isotope analysis of a given sample is
603 typically about ± 0.001 (absolute 2σ). Compositions are normalized to values⁵⁴ for NIST 981 Pb.

604 The Sr, Nd, and Hf fractions of the same sample and standard digestions used for Pb isotopes
605 were further processed at the University of South Carolina, but we note that Pb isotope data for
606 sample EX1606-D3-3 were collected at the University of South Carolina via methods similar to
607 those used at UH and normalized to accepted NIST 981 values⁵⁵. Sr samples were purified with
608 Sr-Spec resin in HNO₃. For Nd, the REE fractions were separated from major element matrix via
609 TRU-spec resin in HNO₃ and HCl media, and Nd separated from the other REE on an LN-resin
610 using 0.25N HCl. Hf was isolated from the matrix on LN resin from the fractions recovered from
611 the washes of the TRU spec column⁵⁶. A ThermoFinnegan NeptunePlus at University of South
612 Carolina was used for remaining (Sr, Nd, and Hf⁵⁷) isotope analyses. Repeated analyses of
613 SRM987 dispersed with the samples gave $^{87}\text{Sr}/^{86}\text{Sr} = 0.710321 \pm 0.000007$, (2σ , $n=11$). The data
614 are reported relative to the recommended SRM987 $^{87}\text{Sr}/^{86}\text{Sr}_{\text{SRM987}} = 0.71025$. Nd isotopes were
615 corrected for fractionation using $^{146}\text{Nd}/^{144}\text{Nd} = 0.7219$ and repeated analyses of the JNdi-1
616 reference material yielded an average $^{143}\text{Nd}/^{144}\text{Nd} = 0.512102 \pm 0.000005$ (2σ , $n=11$). The Nd
617 data are reported relative to the accepted value for JNdi-1 of $^{143}\text{Nd}/^{144}\text{Nd} = 0.512115$. Hf isotopes
618 were corrected for fractionation using $^{179}\text{Hf}/^{177}\text{Hf} = 0.7325$. An in-house Hf standard solution
619 was determined at $^{176}\text{Hf}/^{177}\text{Hf} = 0.282142 \pm 0.000006$ (2σ , $n=8$), which corresponds to the
620 original JMC 475 solution value of $^{176}\text{Hf}/^{177}\text{Hf} = 0.282163$. The data are reported relative to the
621 accepted JMC 475 value of $^{176}\text{Hf}/^{177}\text{Hf} = 0.282160$ ⁵⁸. BCR-2 duplicates are duplicate analyses
622 of the same digestion.

623 Results and brief sample characterizations, including age-corrected isotopic ratios for the Wake
624 samples based on successful age determinations (see next section for details), are reported in the
625 Supplementary Data Table 1. Six of the samples reported here are consistent with the
626 interpretation that they originated from the Rurutu-Arago hotspot. The seventh sample (D13-1)
627 has an age of 164 Ma (Supplementary Data Table 3) is too old to have originated from the

628 Rurutu-Arago hotspot by ~70 Myr and is more likely related to seafloor formation. Isotopic
629 behavior shown in Extended Data Fig. 8 and Extended Data Fig. 9 demonstrate the
630 compositional agreement between the new samples characterized here, and published data for the
631 Rurutu-Arago hotspot track.

632 **Sample analysis for $^{40}\text{Ar}/^{39}\text{Ar}$ geochronology**

633 $^{40}\text{Ar}/^{39}\text{Ar}$ age determination experiments were conducted at the Oregon State University Argon
634 Geochronology Laboratory using incremental CO_2 laser heating in conjunction with multi-
635 collector noble gas mass spectrometry. Preferred lava flow samples were chosen based on
636 petrographic analyses, focusing on phenocryst abundances and relative degree of alteration.
637 Samples that contained fresh phenocrystic phases (clinopyroxene and plagioclase) were
638 preferentially chosen. In the absence of phenocrysts, groundmass was selected for $^{40}\text{Ar}/^{39}\text{Ar}$
639 analyses. When available, multiple phases from a single lava flow were analyzed to test for age
640 reliability. Rocks were crushed and sieved to grain size fractions of 100-180 μm for the most
641 altered samples and 180-250 μm for fresher and coarser phenocryst phases. These fractions were
642 washed in deionized water and dried in a 50°C oven overnight. Following, target phases were
643 concentrated using a Frantz magnetic separator. The crushate were then leached with 1-hour
644 sonic baths in 1N HCl, 6N HCl, 1N HNO_3 and 3N HNO_3 with thorough rinsing and sonication in
645 deionized water between each bath. Plagioclase was subsequently leached twice in 5% HF for 5
646 minutes and clinopyroxene samples were additionally leached once in 15% HF for 15 minutes.
647 The groundmass crushate was divided into three aliquots: 1. no HF treatment; 2. 5% HF for 90
648 seconds; 3. 5% HF for 3 minutes. All samples were then sonicated in ultrapure water for 1 hour.
649 Samples were dried at 50°C in an oven overnight then handpicked under a binocular microscope
650 to achieve pure and homogeneous mineral separates.

651 Approximately 2 to 50 mg of each separate was packed into aluminum capsules for irradiation.
652 Fish Canyon Tuff sanidine was used as a flux monitor loaded at the bottom, top and between
653 every three sample packets. The sample columns were irradiated for 6 hours in the CLICIT
654 position of Oregon State University's TRIGA nuclear reactor. Incremental heating experiments
655 consisted of 20-30 steps for phenocrysts and 50-60 steps for groundmass separates. Blanks were
656 measured at the beginning, end, and every 2-3 incremental heating steps.

657 Experiments consisted of loading 2-25 mg of individual samples into a copper tray, which were
658 then brought under an ultra-high vacuum. Samples were pre-cleaned using a defocused 30W
659 Synrad CO₂ laser beam at low power to release adhered atmospheric gas. Separates were then
660 heated by scanning the CO₂ laser beam over the separates for 60s using incrementally higher
661 laser power. Gas was processed using three getters held at ~450°C, 250°C and 20°C for a total of
662 3-minutes for plagioclase and 6-minutes for clinopyroxene and groundmass. Five masses were
663 analyzed simultaneously using a Thermo Fisher Scientific™ multi-collector ARGUS-IV mass
664 spectrometer with 40, 39, 38 and 37 measured in 1013-ohm Faraday cups, and 36 was measured
665 on an ion-counting CuBe electron multiplier. Ages were calculated using ArArCALC v2.7.0⁵⁹.
666 All ages are normalized to Fish Canyon Tuff sanidine age of 28.201 ± 0.046 Ma (2σ) using the
667 decay constant of $5.530 \pm 0.097 \times 10^{-10}$ yr⁻¹ (2σ)^{60,61}. Air standards were analyzed to obtain mass
668 discrimination factors using an atmospheric ⁴⁰Ar/³⁶Ar of 298.56 ± 0.31 (0.104%)⁶². Refer to Age
669 Results (next section) for other correction factors used during sample calculations.

670 Age Results

671 Four of the seven samples reported in this study were chosen for ⁴⁰Ar/³⁹Ar age determination
672 experiments based on petrographic analysis: EX1606-D3-3, EX1606-D10-1, EX1606-D12-1,
673 and EX1606-D13-1. The remaining 3 samples were not suitable for age determination based on
674 examination of thin sections. Age determinations are interpreted to be eruption ages because
675 each mineral phase used was a primary phenocryst within the sample. Here we determine if an
676 age experiment is concordant if it incorporates 50% or more of the cumulative ³⁹Ar% released
677 within the plateau and the steps are reasonably concordant provided the age and alteration state
678 of the submarine lava flows. For phases with more than one experiment, ages are stacked such
679 that the individual heating steps are combined into one large experiment. EX1606-D10-1 and
680 EX1606-D12-1 did not produce age determination in line with community guidelines, and thus
681 are not considered here. However, phenocryst separates from EX1606-D3-3 and plagioclase
682 separates from EX1606-D13-1 produced reliable eruption age determinations (Extended Data
683 Figure 11 A-F).

684 Plagioclase separates from EX1606-D3-3 yielded a plateau age of 91.21 ± 0.17 Myr (2σ ; n=2)
685 (Extended Data Figure 11A). The inverse isochron indicates ⁴⁰Ar/³⁶Ar_{initial} of 287.51 ± 33.77 ,

686 within uncertainty of atmospheric values (298.56^{62}). Correspondingly, the inverse isochron and
687 plateau age determinations are within error of one another. The plateau age of the clinopyroxene
688 separate from the same sample (91.68 ± 14.61 Ma-2 σ ; n=1) (Extended Data Figure 11C) agrees
689 with the plagioclase age determination but has high uncertainty due to low K-abundance. One
690 step in both the clinopyroxene and plagioclase experiments suggest anomalously low ages,
691 which are likely the degassing of a melt inclusion and not representative of eruption timing.
692 Since the plateau is continuous prior-to and after the heating step with anomalous apparent ages,
693 they are excluded from the plateau calculation. While we prefer the plagioclase age
694 determination due to high-resolution, an age of 91 Ma is further supported by the clinopyroxene
695 age determination.

696 Plagioclase separates from EX1606-D13-1 yielded a plateau age determination of 164 ± 0.29 Ma
697 (2σ ; n=1) (Extended Data Figure 11D). The inverse isochron age (163.72 ± 0.23 Ma; n=1)
698 (Extended Data Figure 11E) is within error of the plateau age determination ($^{40}\text{Ar}/^{36}\text{Ar}_{\text{initial}}$: 308
699 ± 33.44). The three groundmass separates from D13-1 (Extended Data Figure 11F) produced age
700 spectrums that do not meet the statistical criteria for a reliable age determination⁶³ but generally
701 support the Middle Jurassic age inferred from the corresponding concordant plagioclase separate.

702

703 **Color-coding**

704 In order to show the compositional distinction between the hotspot tracks in the western Pacific,
705 as well as to show how compositions backtrack around present-day hotspots, the radiogenic
706 isotope composition of the tracks are color-coded^{14,17,44}. The technique focuses on use of
707 $^{87}\text{Sr}/^{86}\text{Sr}$ - $^{143}\text{Nd}/^{144}\text{Nd}$ - $^{206}\text{Pb}/^{204}\text{Pb}$ isotope compositions, because principal component analysis
708 shows these represent the largest compositional variations in hotspots^{64,65}. In this space, hotspots
709 scatter between four extreme end-member compositions: HIMU, EMI, EMII, and DMM⁶⁶. Each
710 hotspot's samples define an elongated, prolate ellipsoid, and these ellipsoids (32 in the global
711 hotspot database) radiate from a central region, known as FOZO⁶⁵ or C⁶⁷. The color-coding⁴⁴
712 assigns a level of color-saturation based on its distance from this center, while the color depends
713 on the end-member that a particular sample trends closest to (Fig. 1 inset). Compositions that are
714 on the trend toward an end-member, but cannot be resolved from the central FOZO⁶⁵ or C⁶⁷

715 component are colored grey (note that the cutoff percentages for each end-member are shown on
716 colorbars in the Fig. 1 inset). Using this color-coding approach results in a “blue” color for
717 symbols, representing HIMU compositions, which dominate hotspot track that run from the
718 Cook-Austral Islands in the central equatorial Pacific to seamount tracks in the Western Pacific.
719 This HIMU compositional “signature band” in map view (i.e., as the blue symbols the represent
720 the Rurutu-Arago HIMU hotspot track form a “band” across the south Pacific and into the
721 Western Pacific Seamount Province) is consistent with predicted absolute plate motion (APM) in
722 the Pacific until at least 80 Ma, and forms the basis for our investigation that links the Wake area
723 seamounts in the Western Pacific to the long-lived Rurutu/Arago hotspot that also includes the
724 Tuvalu islands and the Gilbert Ridge seamount track. In addition, the red (representing EM2) and
725 green (EM1) compositional color coding for Samoa appears in young Samoan hotspot lavas and
726 also appears in the far western Pacific in the Cretaceous Magellan seamounts. Recent work in
727 Samoa has shown a temporal compositional evolution from red (EM2) to green (EM1),
728 representing the evolution from shield to rejuvenated stage of volcanism at Samoa, and the same
729 is observed in the Western Pacific when compositions and ages are assessed (Hemler and
730 Vlinder seamounts^{4,68}; Extended Data Fig. 5).

731 **Absolute Plate Motion Modeling**

732 Although initial models^{2,69} already showed that simple plate rotations do fit the shapes of several
733 hotspot tracks, recent models³⁹ have evolved to include more sophisticated techniques to find the
734 best-fit absolute plate motion models by using multiple hotspots and by resolving continuous
735 plate rotations from both seamount locations and ages. In addition, some models include large
736 scale mantle flow, comparisons between ocean basins, and plume motion^{6,38,70}. For the Pacific
737 plate >80 Ma, little data are available as neither Hawaii nor Louisville continue past 80 Ma^{71,72},
738 and plate circuits that would allow comparison with the Indo-Atlantic hotspot do not extend
739 beyond this time either⁶. In most existing models, the time period prior to 80 Ma is populated
740 with data from Shatsky Rise and the Mid-Pacific Mountains, yet their respective structures were
741 within ~1,000 km of the ridge system⁶⁷⁷³ (Extended Data Fig. 1) and during their formation these
742 tracks are likely to have been influenced by ridge interaction^{35,73}. However, the Rurutu-Arago
743 and Samoa hotspots do define tracks in this age range that are clearly distinct in their isotopic
744 compositions (Fig. 1; see Section on Color Coding) and that are truly intraplate prior to 80 Ma

745 (Extended Data Fig. 1). We conclude that Rurutu-Arago and Samoa therefore are a more faithful
746 reflection of APM for the Pacific plate.

747 The presence of two hotspot tracks—Samoa and Rurutu-Arago—provides a means to fit a plate
748 rotation for 80-100 Ma that fits both hotspots, thereby relying on their common motion to define
749 an APM pole for that period. Unlike younger volcanic tracks, Samoa and Rurutu-Arago provide
750 enough data to outline the overall hotspot track; however, the sample and data density are low,
751 such that constraints are lacking for a high-resolution model³⁹. Instead, the available data here
752 are used to identify an 80-100 Ma section in both volcanic tracks (Extended Data Fig. 6;
753 Extended Data Tables 1, 2), after which a least-squares method is used to find the best-fit
754 rotation pole for both hotspots. The method¹⁸ consists of finding the best-fit pole that minimizes
755 the variance in calculated angular (seamount-pole) distances, in the least-squares sense. The
756 solution is found with a grid-search algorithm that tests

$$757 \quad \text{var}(d_{ij}) = \sum_{j=1}^M \sum_{i=1}^N \frac{(d_i^j - d_{mean}^j)^2}{N}$$

758 which calculates the variance in distance (d) for all seamounts in the 80-100 Ma track segment
759 relative to the mean distance for a given hotspot (d_{mean}). The variation in distance per hotspot is
760 normalized by the number of seamounts (N) per hotspot. This technique suggests a best-fit stage
761 pole west of the Samoa-related seamounts, near the equator (0.7°S, 315.7°E, rotation rate:
762 0.975°/Myr; Extended Data Table 1). The resulting K01m APM model is a much better fit to the
763 two hotspot tracks, particularly for the Rurutu-Arago hotspot, where the predicted track now
764 bends to the west at ~100 Ma, just northwest of Wake Island (Fig. 1, Extended Data Fig. 4, 5).
765 Due to the shift in the rotation pole compared to prior models, the angular distance from the pole
766 to the Rurutu-Arago track and the new rotation rate provide a better fit to the seamount track.
767 Despite these improvements, several issues must be considered before the new model can be
768 applied to the Louisville hotspot track.

769 Plate motion southeast of OJP involved more than just the Pacific plate. During the break-up of
770 OJP-Nui, the Manihiki and Hikurangi plates formed, while the Chazca plate resided immediately
771 to the east⁴⁹. It is important to evaluate whether these plates moved independently with respect to
772 the Pacific plate while the Ellice Basin was located over the Louisville hotspot. The relevant

773 plates/microplates are associated with the break-up of OJP-Nui. The oldest Louisville Seamounts
774 (ranging in age from 1 to 79 Ma^{8,36}) are located south of the Osbourn Trough and west of the
775 Wishbone Scarp, representing a small plate forming as Hikurangi separated from OJP. However,
776 true spreading on the Osbourn Trough may have ceased between 101-100 Ma^{74,75}. Any further
777 rotation of this plate ceased between ~84 Ma-79 Ma^{76,77}, so Louisville Seamounts younger than
778 79 Ma formed after this plate was already part of the Pacific plate. Thus, Louisville Seamounts
779 after 79 Ma properly represent Pacific plate motion with respect to the Louisville hotspot. The
780 only other area where older volcanoes related to Louisville may be exposed is in the area of the
781 Ellice Basin between OJP and Manihiki¹⁴. However, the exact timing of cessation of motion
782 between the separating plateaus is not well constrained²¹. The sparse age information from the
783 Ellice Basin includes the 95 Ma Foumatua seamount located on the fossil ridge system¹⁴,
784 constraining a minimum age of ~95 Ma for when seafloor spreading in the Ellice Basin shut
785 down, as suggested by models based on seafloor fabric⁷⁸. Critically, Foumatua Seamount is part
786 of a group of similarly aged “Ellice Basin Seamounts” that have an isotopic composition that
787 overlaps with that of the younger Louisville Seamounts¹⁴ (Fig. 2). These seamounts are located
788 where our APM model predicts the Louisville hotspot around ~95 Ma, and the seamounts are
789 also age-progressive with the Louisville seamounts (Fig. 1, 2). The 115 Ma Seka Seamount,
790 located north of the Ellice Basin fossil ridge and near the southern terminus of Gilbert Ridge
791 several hundred kilometers east of the OJP, places the underlying seafloor – and westward
792 motion of the OJP fragment relative to the plume – at a minimum age of 115 Ma, thus indicating
793 that early stage Ellice Basin opening was rapid, and potentially even triggered by the voluminous
794 melting of the Louisville plume head at that time, much like the inferred fossil plume head-ridge
795 system at TAMU Massif³⁰.

796 Due to the known wide variation in paleomagnetic latitude estimates for OJP⁵⁰, any microplate
797 considerations prior to ~100 Ma are under constrained at best. Either the plateaus rotated around
798 the time of break-up⁵⁰, or OJP was already fixed with respect to the Pacific plate⁷⁷. Regardless,
799 the sheer size of the entire Ontong Java Nui combined structure is so large that neither a rotation
800 of the plateaus, nor ongoing spreading in the Ellice Basin until ~100 Ma, would place the
801 predicted Louisville hotspot outside of the outline of the combined OJP-Nui plateau (or even
802 OJP by itself) at 120 Ma (Fig. 3). This is mainly due to the final east-west length of the 100-120

803 Ma predicted Louisville hotspot track being shorter than the width of OJP, which is thought to
804 have largely moved east-west^{21,78} (Fig. 1). In Fig. 3, the approximate eruptive locations are also
805 shown assuming OJP either was fixed from ~120 Ma, or only rotated around a pole internal to
806 the plateau⁵⁰. Intriguingly, the rotation of the plateaus places the eruptive location at ~120 Ma
807 near the triple junction between the three plateaus.

808 **Backtracking**

809 Individual volcanoes with age determinations can be backtracked to their original eruptive
810 location, by rotating present-day volcano locations in the opposite direction of plate motion
811 according to the sequence of APM model rotations. Existing APM models are used as stage pole
812 rotations to accommodate volcanic ages in between supplied finite rotations. Instead of each
813 volcano backtracking to the same single hotspot location, this process generates clusters due to
814 various geologic and measurement uncertainties, such as: (1) volcanic age precision and
815 accuracy, (2) extended eruption of single volcanoes (up to 7 Ma⁷⁹), (3) offset between sampled
816 rift zone eruptions and the central crater, and (4) lithospheric structure offsetting volcano from
817 mantle source^{4,80}. Cumulatively, these uncertainties could cause hundreds of km of scatter in
818 backtracked locations that cluster around the present-day hotspot⁴⁴.

819 Two categories of structures were backtracked here: (1) individual volcanoes of Rurutu-Arago,
820 Samoa and Louisville, and (2) the OJP as a single structure. For the individual hotspot volcanoes
821 (Extended Data Table 2), published ⁴⁰Ar/³⁹Ar ages were used^{9,81-85}, while symbols for
822 reconstructed volcanoes are colored (see Color-Coding) based on their isotopic composition<sup>10-
823 12,14,43</sup>. This highlights the compositional groups by color, matching present-day hotspot locations
824 at Samoa and Rurutu-Arago, as well as Macdonald and Rarotonga for reference. Moreover, the
825 probability density function of backtracked locations (constructed with a Gaussian kernel) shows
826 four peaks in the distribution that also correspond to the same four present-day hotspots
827 (Extended Data Fig. 5). In addition to the density estimates, a running mean can also be
828 calculated for the backtracked locations and related sample ⁴⁰Ar/³⁹Ar ages. These “age tracks”
829 represent a smoothed estimate of how the hotspot source moved in time, with respect to the
830 applied APM model, which can be thought of a proxy for plume motion in that reference frame.
831 The results for the various models emphasize the tighter scattering (in blue HIMU-composition

832 around Rurutu-Arago, red-green around Samoa) and shorter plume motion tracks for the new
833 K01m model. This result implies the least amount of plume motion is required for these models,
834 while models that allow for plume motion require a significant amount, but also match predicted
835 plume motion^{6,70} back to ~50 Ma for Hawaii and Louisville (Extended Data Fig. 5). Since there
836 are no plate circuits >80 Ma to enable comparison to the Indo-Atlantic hotspot reference frame³⁸,
837 the modeling results can only be tested against Pacific hotspots.

838 While testing the model against Rurutu-Arago and Samoa constraints is potentially circular,
839 backtracking the OJP constitutes a more interesting test, as it was previously shown to backtrack
840 1,200 km away from the closest hotspot at 120 Ma, i.e., Louisville¹. By defining the outline of
841 the plateau as a series of individual points⁸⁶, each individual point is backtracked with the
842 updated K01m APM model. The result shows that the backtracked OJP plateau outline is located
843 directly over the present-day Louisville hotspot (Extended Data Fig. 5). Similarly, the
844 backtracked individual Louisville seamounts are also located over the present-day Louisville
845 hotspot. The updated K01m model thus resolves the north-south discrepancy between modeling
846 predictions of the eruptive location of the OJP and the track of Louisville. The conclusions for a
847 120 Ma OJP formation also hold for a slightly younger age of formation, recently suggested to
848 be ~116 Ma⁵¹. In this case, the modeled Louisville hotspot and Eastern Salient of the OJP are
849 still closely spatially associated with each other at ~116 Ma. The revised OJP formation age is
850 similar to that of Seka Seamount, which would further suggest that OJP-Nui formation and
851 initiation of Ellice Basin rifting were simultaneous events. This model represents a fixed hotspot
852 model, while multiple lines of evidence suggest hotspot sources to be mobile⁵. However, motion
853 estimates for Louisville hotspot are within error of its location until at least ~70 Ma^{8,9}, and older
854 data for greater Ontong-Java Nui are too variable to constrain any possible plume motion.
855 Regardless of a lack of tight paleolatitude constraints, the size of greater Ontong-Java Nui allows
856 for hundreds to thousands of kilometers of plume motion superimposed on our new model, while
857 still maintaining the “end” of the Louisville hotspot track within its outline.

858 SUPPLEMENTAL MATERIAL

859 Background Data Sources for Fig. 1

860 Most of the previously published data used in Fig. 1 were sourced from GEOROC
861 (<https://georoc.eu/>) precompiled files for ocean islands and seamounts, which were filtered to
862 remove sample data known to be affected by contaminants and/or analytical problems. Non-
863 igneous lithologies were also filtered out. Additional isotope and/or geochronological data were
864 compiled for the Northwest Hawaiian Ridge⁸⁷⁻⁸⁹, Vlinder Seamount⁹⁰, Arago Seamount⁹¹, and
865 Moki Seamount and Rose Atoll⁹².

866

867 **Isotope data groupings used in Fig. 2**

868 The isotopic compositional range spanned by the plateau and smaller structures follow a
869 general temporal pattern. The East Pacific Rise field⁹³ is given for comparison. The majority of
870 the plateau data from OJP, MP, and HP plots between EM1⁶⁶ and a central geochemical
871 component, like FOZO⁶⁵. The OJP data⁹⁴⁻⁹⁷ consist of the major basement Kwaimbaita and
872 Kroenke components, which represent a relatively high degree of mantle melting with a
873 composition between EM1-FOZO, while the Singgalo component represents a later phase of
874 plateau construction, with a more EM1-rich composition⁹⁸ during the LIP stage of the plume.
875 These OJP stages are shown as red fields in Fig. 2, and they are followed by a much later and
876 smaller ~91 Ma alkalic stage⁹⁵ (Sigana Formation) that shifted to HIMU⁶⁶ compositions (pink
877 field in Fig. 2) in the later stages of OJP activity. Data from MP show basement rock
878 compositional groups similar to the Kwaimbaita/Kroenke and Singgalo lavas at OJP, but
879 recognized⁹⁹ as high-Ti EM1-type lavas (dark orange field in Fig. 2), while low-Ti lavas have
880 FOZO-type compositions incorporating potentially a small amount of a HIMU-type source (light
881 orange field in Fig. 2). This HIMU component is also argued to be the primary source for MP
882 late-stage lavas, just as it is at OJP; similarly at HP, the EM1-FOZO main plateau lavas (dark
883 purple, Fig. 2) are followed by the late stage HIMU HP Seamounts^{28,95,98,100} (light purple, Fig. 2).
884 Essentially, EM1-FOZO melts were dominant during the voluminous plateau-building stages,
885 while the later, less voluminous stages of volcanic activity shifted to dominantly HIMU-FOZO
886 melts. It is this full range of compositions and transition from plume head (plateau-building) to
887 plume tail (seamount chain-forming) activity that provides the critical context for the potential
888 chemical connection between Louisville Seamounts and OJP-Nui lavas²⁸, as well as the Ellice
889 Basin seamounts.

890 Given the well-known challenges involved in linking plateau-forming and seamount-
891 forming phases of mantle plume activity using plate motion models, the Ellice Basin Seamounts
892 and Seka Seamount offer an alternative approach: Their proximity to the OJP and their 90-115
893 Ma age range provide evidence of a temporal relationship to OJP-Nui (and specifically the OJP),
894 while representing smaller, seamount-forming stages of volcanic activity more directly
895 comparable to the Louisville hotspot track than the plateau-forming melts. The observation that
896 the 90-115 Ma Ellice Basin and Seka seamounts follow the Louisville age progression (Figure 2)
897 and fill in a critical gap along the age progression between Louisville (1 to 79 Ma) and OJP (120
898 Ma) lends strong support to the hypothesis that these seamounts provide the “missing link”
899 between the Louisville hotspot and OJP.

900 Ellice Basin Seamounts and Seka Seamount exhibit varying degrees of seawater U
901 enrichment consistent with patterns identified in some Jurassic Pacific MORB¹⁰¹. This alteration
902 affects uraniumogenic ²⁰⁶Pb and to a lesser extent ²⁰⁷Pb, but not thorogenic ²⁰⁸Pb as Th is largely
903 immobile during low-T alteration processes. Thus, seawater U alteration is detectable when
904 samples plot right of the Northern Hemisphere Reference Line (NHRL) in ²⁰⁸Pb/²⁰⁴Pb versus
905 ²⁰⁶Pb/²⁰⁴Pb, which over time develops into a broadly horizontal array away from analogous
906 unaltered samples that have retained their primary isotopic composition (Fig. 2). In ²⁰⁷Pb/²⁰⁴Pb
907 versus ²⁰⁶Pb/²⁰⁴Pb, however, affected samples will plot close or slightly under the NHRL, with
908 ingrowth following an isochron consistent with the time of alteration (Fig. 2, top right panel).
909 The Pb isotopes for samples affected in this manner may, however, remain under-corrected after
910 age correction (i.e., they will be more radiogenic than the mantle source). This is because the
911 measured U/Pb abundances of lightly leached sample used for trace element compositional
912 analysis may not adequately reflect the true (higher) ingrowth rate reflected by a strongly leached
913 aliquot of the same sample^{101,102}. The Ellice Basin Seamounts scatter right of the FOZO region in
914 ²⁰⁸Pb/²⁰⁴Pb versus ²⁰⁶Pb/²⁰⁴Pb space, while ²⁰⁸Pb/²⁰⁴Pb overlaps with the least radiogenic samples
915 from the Louisville hotspot track^{28,103}. Further, in ²⁰⁷Pb/²⁰⁴Pb versus ²⁰⁶Pb/²⁰⁴Pb, the Ellice Basin
916 samples define an array consistent with a 95 Ma isochron from a median Louisville initial Pb
917 composition (Fig. 2) that intersects with age-corrected Louisville hotspot track samples and thus
918 suggests, despite undercorrection for ²⁰⁶Pb ingrowth, the two groups share a genetic link.

919 The Ellice Basin Seamounts (and Seka) are depleted^{14,44} in $^{143}\text{Nd}/^{144}\text{Nd}$ versus $^{87}\text{Sr}/^{86}\text{Sr}$,
920 resembling varying mixtures of FOZO, HIMU, and DMM consistent with our conclusions about
921 the original Pb isotope composition of the Ellice Basin and Seka seamounts (Fig. 2). The least
922 radiogenic (age-corrected) Ellice Basin-type samples overlap with the most radiogenic
923 compositions in the Louisville hotspot track field, further corroborating a genetic link between
924 the two groups. While some of the samples show decoupling between $^{143}\text{Nd}/^{144}\text{Nd}$ and
925 $^{176}\text{Hf}/^{177}\text{Hf}^{14}$ as a likely consequence of phosphatization processes on Nd isotopic
926 compositions¹⁰², the phosphate-insensitive $^{176}\text{Hf}/^{177}\text{Hf}$ ratios of the Ellice Basin Seamounts also
927 extend from HIMU-like values into more radiogenic, DMM-like values. The Ellice Basin
928 Seamounts are similar in age to crustal ages inferred for the Ellice Basin itself⁷⁸; thus the Ellice
929 Basin Seamount mantle source melted below young, thin lithosphere. As a result, the Ellice
930 Basin seamount melts likely incorporated a larger proportion of a DMM-type component than
931 the younger Louisville seamounts that erupted below older, thicker lithosphere¹⁰³, not unlike
932 increasing proportions of DMM observed in the older stages of the Hawaiian and Louisville
933 hotspot tracks as a function of proximity to a ridge^{104,105} (Extended Data Fig. 9). The
934 combination of 1) overlapping componentry between Ellice Basin and Seka seamounts and the
935 Louisville hotspot track, 2) spatiotemporal proximity of the Ellice Basin and Seka seamounts to
936 the OJP, and 3) excellent agreement of Ellice Basin and Seka to our new APM model
937 reconstruction of the Louisville hotspot track (Fig. 1) and age progression (Extended Data Fig. 8)
938 provide the first robust evidence of the long-proposed link between Louisville and OJP-Nui.

939 **Age corrections to isotope data**

940 Data in Fig. 2 were age corrected to initial isotopic ratios in order to compare isotopic
941 compositions of different temporal groups and/or distinct compositional groups characterized in
942 the OJP, MP, and HP as well as the Louisville hotspot track and Ellice Basin Seamounts. Where
943 possible, ages obtained on specific samples were used to correct their isotopic ratios; for suites
944 with known age constraints, recommended age estimates²⁸ were used for samples without age
945 determinations. Parent-daughter (P/D) ratios used to calculate the time-integrated ingrowth
946 relative to ^{204}Pb were determined from trace element data and using decay constants of
947 $1.55125 \times 10^{-10} \text{ yr}^{-1}$ for ^{238}U , $9.8571 \times 10^{-10} \text{ yr}^{-1}$ for ^{235}U , and $4.948 \times 10^{-11} \text{ yr}^{-1}$ for ^{232}Th .

948 All isotope data for the new Wake samples were also age-corrected using the same decay
949 parameters as for the Louisville data. For all samples except EX1606-D13-1, an age of 91 Ma
950 (based on a successful age determination from this seamount, located near the other seamounts
951 discussed in this study), was assumed for six of the seven seamounts to simulate a reasonable
952 estimate of initial ratios. Initial ratios did not shift significantly enough to change interpretations
953 for any of the lavas when calculated for 100 or 80 Ma. Sample EX1606-D13-1 was age-corrected
954 to 164 Ma based on new $^{40}\text{Ar}/^{39}\text{Ar}$ analyses of plagioclase separates, reported at the end of the
955 Supplement. Initial ratios were then forward-modeled to present-day ratios using estimates of
956 parent-daughter ratios of the HIMU mantle source for Pb, Nd, and Hf isotopes¹⁰⁶ and (because
957 Nebel et al.¹⁰⁶ do not provide Rb/Sr ratios) primitive mantle parent-daughter ratios for Sr
958 isotopes¹⁰⁷, following parameters of an identical exercise¹⁴. These data are reported in
959 Supplementary Data Table 1.

960 For most of the new Wake samples, age-corrections to $^{87}\text{Sr}/^{86}\text{Sr}$, $^{206}\text{Pb}/^{204}\text{Pb}$, and
961 $^{143}\text{Nd}/^{144}\text{Nd}$ isotope ratios are large, producing initial isotopic ratios significantly less radiogenic
962 than expected for the modern mantle source. Forward-modeling those initial ratios back to
963 present-day estimates, however, produces model ratios comparable to most of the measured
964 sample data (Supplementary Data Table 1). Prior modeling on 100 Ma alkali ocean island basalts
965 found similar disagreement between age-corrected and modern isotope ratios, particularly when
966 parent-daughter ratios are high (e.g., Pb isotopes in HIMU melts), yet also good agreement
967 between forward-modeled and measured ratios¹⁰⁸. This suggests that the utility of age corrections
968 for old alkaline basalts with high P/D ratios may be questionable when the intent is to compare
969 isotopic compositions with their modern counterparts that have undergone little radiogenic
970 ingrowth.

971 Therefore, Figure 1 and Extended Data Figure 9 provide examples of the comparability
972 of non-age corrected (i.e., measured) Cretaceous and modern lavas from the Rurutu-Arago
973 hotspot. Measured $^{143}\text{Nd}/^{144}\text{Nd}$ ratios from Cretaceous parts of the hotspot track, for example,
974 closely resemble $^{143}\text{Nd}/^{144}\text{Nd}$ ratios from the youngest part of the track. Furthermore, trace
975 element data are not available for all previously published isotope data used in this study, and
976 thus age corrections are not possible for all data. For completeness, only measured isotopic ratios
977 are shown in figures discussing seamount geochemistry. The exception is Fig. 2, where a broad

978 range of OJP-Nui-Louisville melts, which represent a range of high and low degree melts and
979 mantle source compositions produced from 120 Ma to present, are shown.

980 **Alteration**

981 Cretaceous seafloor rocks are nearly ubiquitously altered by seawater and various secondary
982 mineralization processes. The abundances of fluid-mobile elements, and correspondingly some
983 parent-daughter ratios of traditional radiogenic isotope systems used to identify mantle sources
984 of intraplate volcanoes, may be modified by these processes. Alternatively, dissolved trace
985 metals in seawater (e.g., Sr, Nd) can overprint the magmatic isotopic signature of a lava. Strong
986 acid leaching is employed to remove secondary isotopic overprints obscuring primary magmatic
987 signatures²⁹. However, cryptic alteration of some isotopes and/or time-integrated primary
988 isotopic ratios resulting from modified parent-daughter ratios may also be present, and cannot be
989 restored via leaching.

990 Trace element ratios such as Th/U and Y/Y* can be used to proxy U mobility and
991 phosphatization processes, respectively. In Extended Data Fig. 10, elevated Th/U correlates with
992 $^{208}\text{Pb}/^{204}\text{Pb}$ of the Wake samples, but no correlation exists with $^{206}\text{Pb}/^{204}\text{Pb}$ (but we note that a
993 lack of correlation is not necessarily related to alteration). Regardless, the new Pb isotopic ratios
994 reported here on Wake lavas are consistent with the range defined by younger segments of the
995 Rurutu-Arago hotspot track (Extended Data Fig. 7), so any isotopic modification by seafloor
996 alteration does not cause the new Wake samples to plot outside of the known Rurutu-Arago
997 isotope field. No correlation with Th/U is apparent with $^{143}\text{Nd}/^{144}\text{Nd}$ or $^{87}\text{Sr}/^{86}\text{Sr}$. When Y/Y* (a
998 proxy for phosphatization) is plotted (Extended Data Fig. 10), the most radiogenic $^{143}\text{Nd}/^{144}\text{Nd}$
999 occurs with the strongest positive Y/Y* anomaly, but no correlation with Pb isotopes is
1000 observed. The same pattern is present in the Ellice Basin Group samples (where characterized for
1001 bulk compositional data¹⁴), suggesting that samples with sufficiently high levels of
1002 phosphatization develop DMM-like $^{143}\text{Nd}/^{144}\text{Nd}$ ¹⁰², which remains unusually radiogenic even
1003 after age correction. Based on trace element evidence, we exclude $^{143}\text{Nd}/^{144}\text{Nd}$ of phosphatized
1004 Ellice Basin and Wake samples from further discussion; data for samples suspected of
1005 phosphatization are shown in plots but are distinguished from the other samples. Ellice Basin

1006 samples lacking bulk composition data are also flagged in relevant figures because the extent of
1007 phosphatization cannot be evaluated for those samples.

1008

1009 **Plate motion history and model shown in Fig. 3**

1010 The exact plate motions of the pieces of greater Ontong Java Nui are still not well
1011 established, however paleomagnetic data of the plateaus, as well as seafloor morphology and
1012 ages between the plateaus has led to different suggestions^{21,50,77,78}. In the scenario where the OJP
1013 was fixed with respect to the Pacific Plate around ~120 Ma, the new model predicts an ~120 Ma
1014 eruptive location on the north side. Alternatively, the plateaus rotated around the time of break-
1015 up around a rotation axis internal to OJP⁵⁰, and the 120 Ma Louisville eruptive location would be
1016 approximately central between the three plateaus that separated. Critically, when employing our
1017 new absolute plate motion model, the large size of greater Ontong Java Nui contains the original
1018 eruptive location of Louisville, regardless of the uncertainties regarding these motions. By ~95
1019 Ma, HP had rifted south, and the Ellice Basin between OJP and MP had mostly opened⁷⁷. The
1020 oldest Ellice Basin Seamount (95 Ma) is located on the fossil ridge^{14,78} and thus defines a
1021 minimum age for final Ellice Basin spreading. An older seamount (Seka, 115 Ma⁴⁴), located near
1022 the southern Gilbert Ridge, has a similar isotopic composition to the Ellice Basin Seamounts and
1023 is likely genetically related (Fig. 2), a hypothesis supported by the observation that Seka both lies
1024 on the new reconstructed hotspot track for Louisville and lies on the Louisville age progression.
1025 The presence of this seamount further supports early, rapid opening of the Ellice Basin by the
1026 time the main plateau-forming phase of OJP-Nui was waning. By this time, MP had been
1027 captured by the Pacific plate⁷⁷, so a Louisville track prediction using Pacific plate motion is
1028 appropriate. Around ~90 Ma, the exact relationship of the Louisville hotspot to the Osbourn
1029 ridge is unclear; volcanoes of this age range have been subducted, and the lack of seafloor
1030 magnetic anomalies around the Osbourn Trough makes establishing exact spreading rates within
1031 a 95-80 Ma time span difficult. However, motion may still have continued on the Osbourn plate
1032 boundary until 79 Ma, after which the entire area was captured by the Pacific plate⁷⁷. At ~79 Ma,
1033 the oldest Louisville seamount^{8,36} erupted south of the Osbourn Trough, so all of the Louisville
1034 seamounts that erupted from that time onward were subjected to Pacific plate motion. Much
1035 later, the Tonga trench experienced roll-back, while the Pacific plate continued to subduct,

This is a preprint of an article that has been submitted to Nature, and revised based on two rounds of peer review, but has yet to be formally accepted for publication.

1036 initiating Louisville Seamount subduction around $\sim 5 \text{ Ma}^{109}$ and continuing today. The “present”
1037 panel of Fig. 3 also shows alternative APM model predictions, all reconstructing south of OJP;
1038 K01¹⁸; WK08³⁹; T19R: model R⁴⁹; T10corr¹¹⁰: subsequently corrected⁴⁹; D12⁶.
1039

1040 **Data availability**

1041 All data generated during this study are included in this published article (and its
1042 supplementary information files), and are available in the EARTHCHEM repository (doi will be
1043 supplied).

1044

1045 **Code availability**

1046 The best-fit plate rotation Matlab code is available upon request from the corresponding
1047 author.

1048 **Author contribution statement**

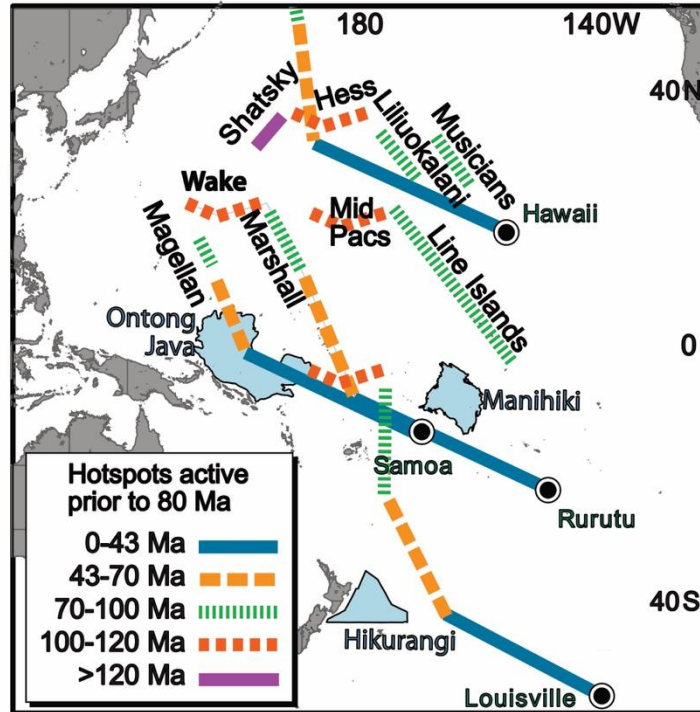
1049 JK and VAF contributed equally to this study. Conceptualization: JK, VAF, MGJ, AAPK. Field
1050 expedition and sampling: CK, JK. Sample preparation and data collection: AA, JK, MB.
1051 Modeling: JK, PW, AAPK. Writing, editing, and figures (original draft): All authors. Writing,
1052 editing, modeling, and figures (revised version): VAF, KK, MGJ, AAPK.

1053 **EXTENDED DATA**

1054 **Extended Data Figures 1- 10**

1055 **Extended Data Tables 1- 2**

1056 **Supplementary Data Tables 1-2**



1057

1058

1059

1060

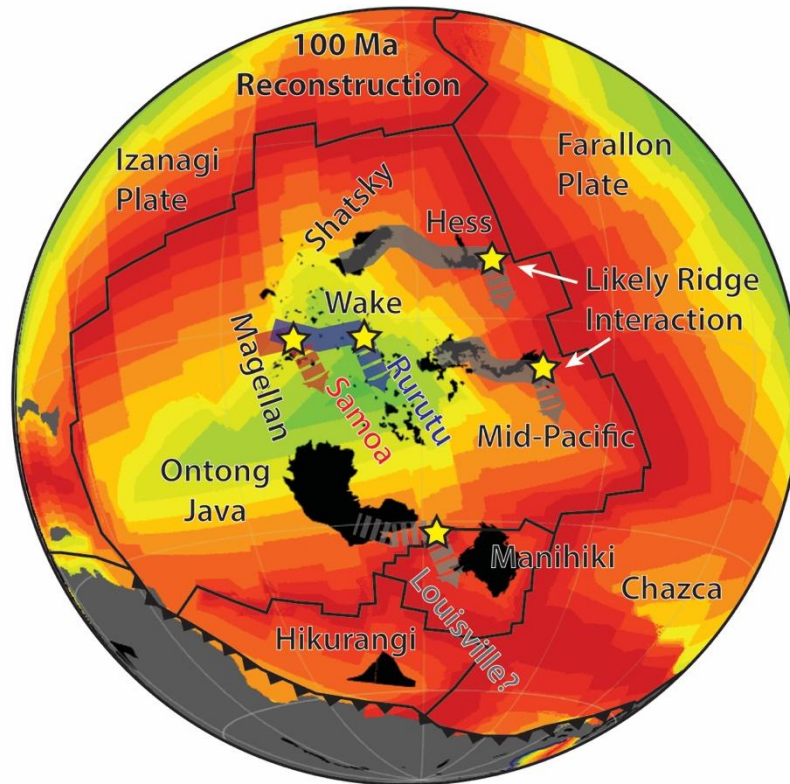
1061

1062

1063

Extended Data Figure 1. Idealized map of the Pacific Ocean basin, showing relevant hotspot tracks, anchored at present-day locations indicated with black dots. Different sections of the hotspot tracks are color-coded by approximate range in eruption ages¹⁸. In the West Pacific, many sections are represented by seamount groups known by their own names. In light blue, the three oceanic plateaus are shown that are thought to have made up Ontong-Java Nui together.

1064

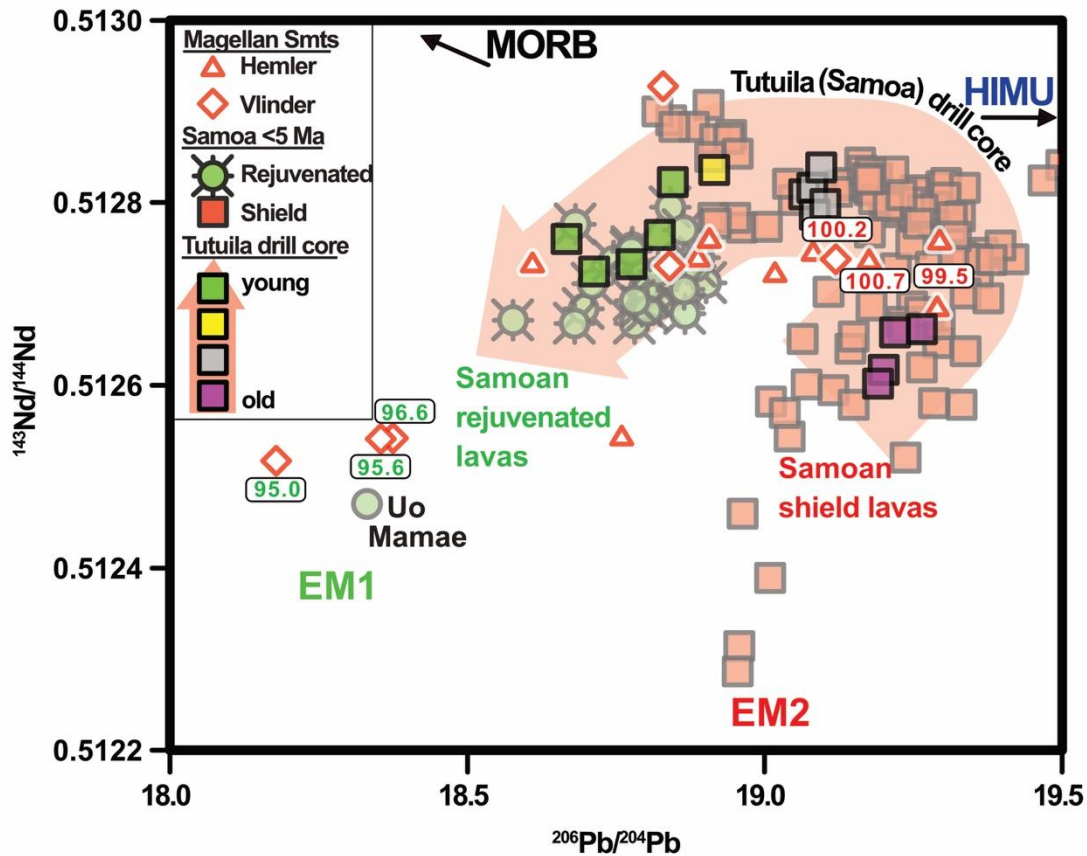


1065

1066 **Extended Data Figure 2.** 100 Ma plate configuration and relative position of volcanic structures
1067 relevant to APM modeling (global projection from GPlates¹¹). Shatsky Rise and Mid-Pacific Mountains
1068 erupted near a spreading center (likely causing plume motion⁵), while Rurutu-Arago and Samoa erupted
1069 within the growing Pacific plate. Louisville's position shows the approximate modeled track for the
1070 updated model rotation.

1071

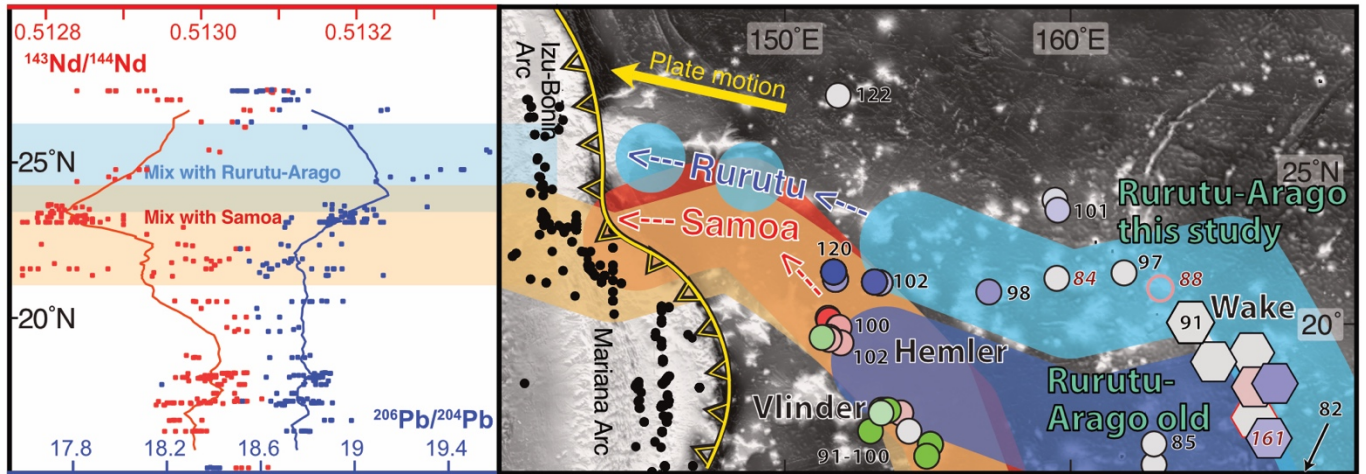
1072



1073

1074 **Extended Data Figure 3.** Compositional overlap between modern Samoa (< 5 Ma) and
1075 Cretaceous Samoan volcanoes—Hemler and Vlinder seamounts—in the West Pacific. Most of
1076 the geochemical evolution of Samoan volcanoes through time is reflected in a drill core into
1077 Tutuila Island (Samoa⁴⁶). This shows (red arrow) a change in lava compositions from shield to
1078 rejuvenated lavas, with volcanoes active over the past 5 Ma⁸². The older samples^{29,68} (ages
1079 shown in white text bubbles) from Hemler and Vlinder (~100 Ma) mainly plot around the shield
1080 lavas in Samoa while the youngest samples (~95 Ma) continue through the rejuvenated lavas
1081 represented by the most extreme EM-1 type composition in the Samoan area (Uo Mamae¹¹²).
1082

1083



1084

1085

1086

1087

1088

1089

1090

1091

1092

1093

1094

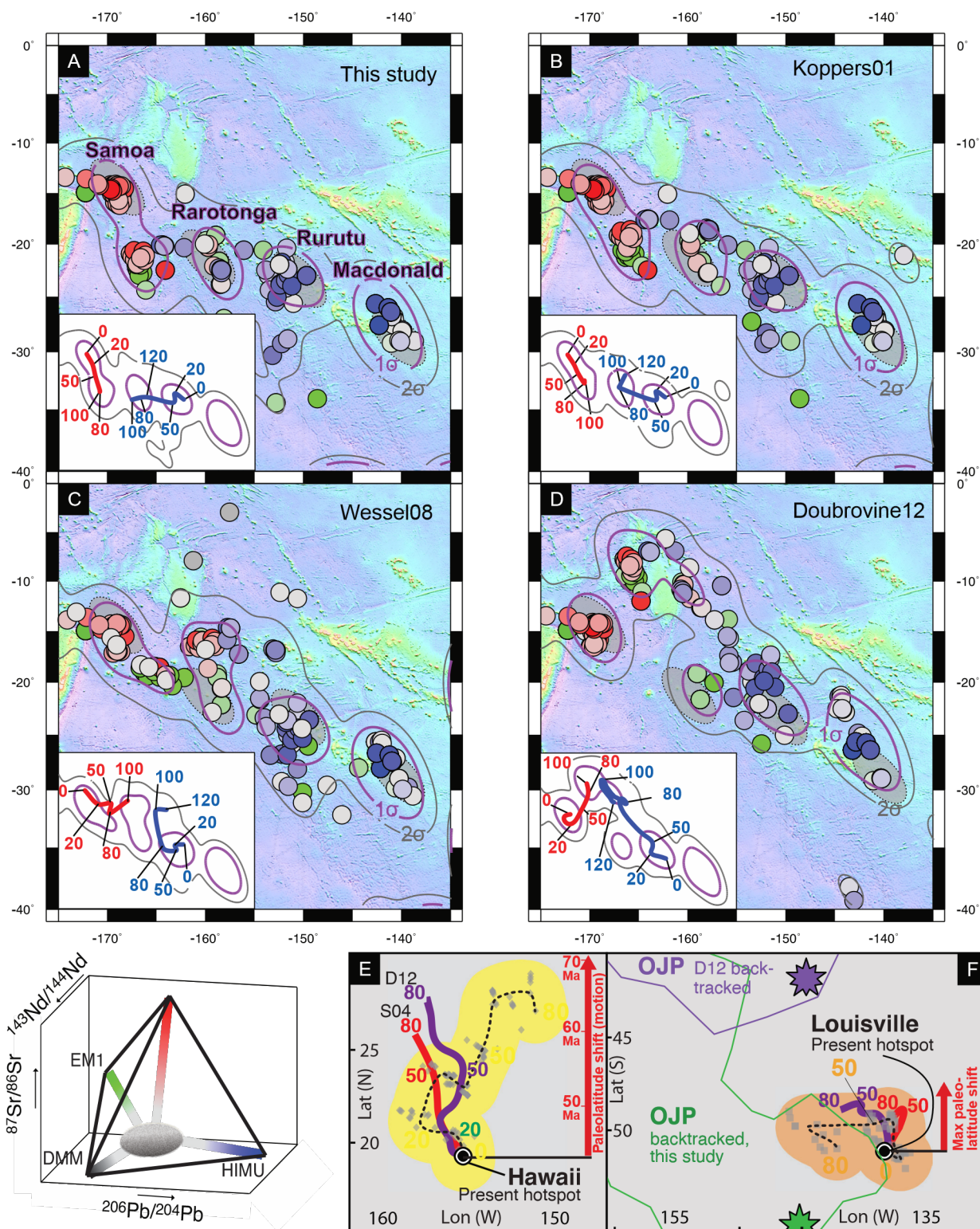
1095

1096

1097

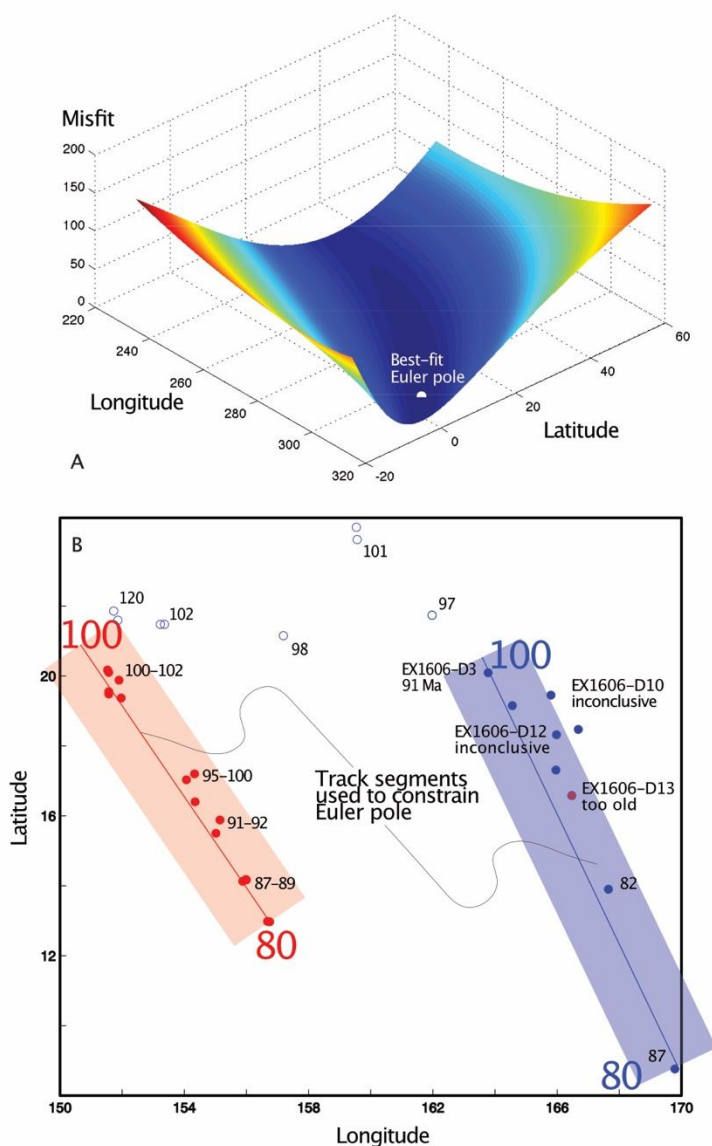
1098

Extended Data Figure 4. Map of West Pacific seamounts, showing Rurutu-Arago and Samoa predicted hotspot tracks (K01¹⁸ in dark shade, this study in light shade). Black numbers with white outline represent ages^{29,83}, while numbers in red represent likely unrelated volcanic ages, given large age difference with expected age along the hotspot track and difference in composition (pink circle²⁹). New Wake region isotope data (hexagons) and a 91.3 Ma age determination provides the “missing link” that suggests that Rurutu hotspot continues through the seamounts west of Wake Island. The samples outlined with red has $^{143}\text{Nd}/^{144}\text{Nd}$ affected by phosphatization. The existing (dark blue¹⁸) APM model track for the Rurutu-Arago hotspot is devoid of major seamounts, while the new track (light blue) continues the unusual isotopic composition and morphological chain to the Izu-Bonin-Mariana trench. A similar prediction for Samoa (red: K01¹⁸; orange: updated) shows both hotspots have a corresponding unusual spike in isotopic compositions in the arc (left panel; lines represent running means), indicating prior subduction of a continuing chain of similar composition, mixing Rurutu-Arago (HIMU) or Samoa (EM2) hotspot material into the mantle wedge.



1099
 1100 **Extended Data Figure 5.** Backtracked original eruptive locations for Samoa and Cook-Austral-related
 1101 volcanoes (Cook-Austral, Samoa, Tuvalu, Gilbert, Wake, Magellan, Tokelau), using various absolute
 1102 plate motion models (a. this study; b. Koppers01¹⁸; c. Wessel08³⁹; d. Doubrovine12⁶). Backtracked
 1103 seamounts color-coded (lower left panel) for their isotopic compositions show that at present-day

1104 hotspots (purple text) are the focus of clusters of consistent geochemical compositions, defined by grey
1105 (2) and purple (1) contours for Gaussian-kernel probability density estimates for the backtracked
1106 locations. Insets show these density contours and the running mean of backtracked location and age to
1107 estimate plume motion from model mismatch from fixed hotspots (a-d). Backtracked (grey symbols⁶)
1108 locations for Hawaii (e) and Louisville (f) and their smoothed age-track (wide yellow or orange)
1109 highlight a deviation from predicted plume motion (S04/red⁷⁰ and D12/purple⁶) beyond 50 Ma,
1110 indicating a mismatch for plate motion models into the Cretaceous. Outlines show Ontong-Java Plateau
1111 (OJP) backtracked with the new model overlap with Louisville, where stars show approximate center of
1112 Ontong-Manihiki-Hikurangi. Red arrows show smoothed tracks match derived latitudinal plume motion
1113 from paleomagnetic latitudes^{13,113}. Backtracking of OJP assumes fixed relationship to the Pacific plate,
1114 with no rotation of the plateau¹.

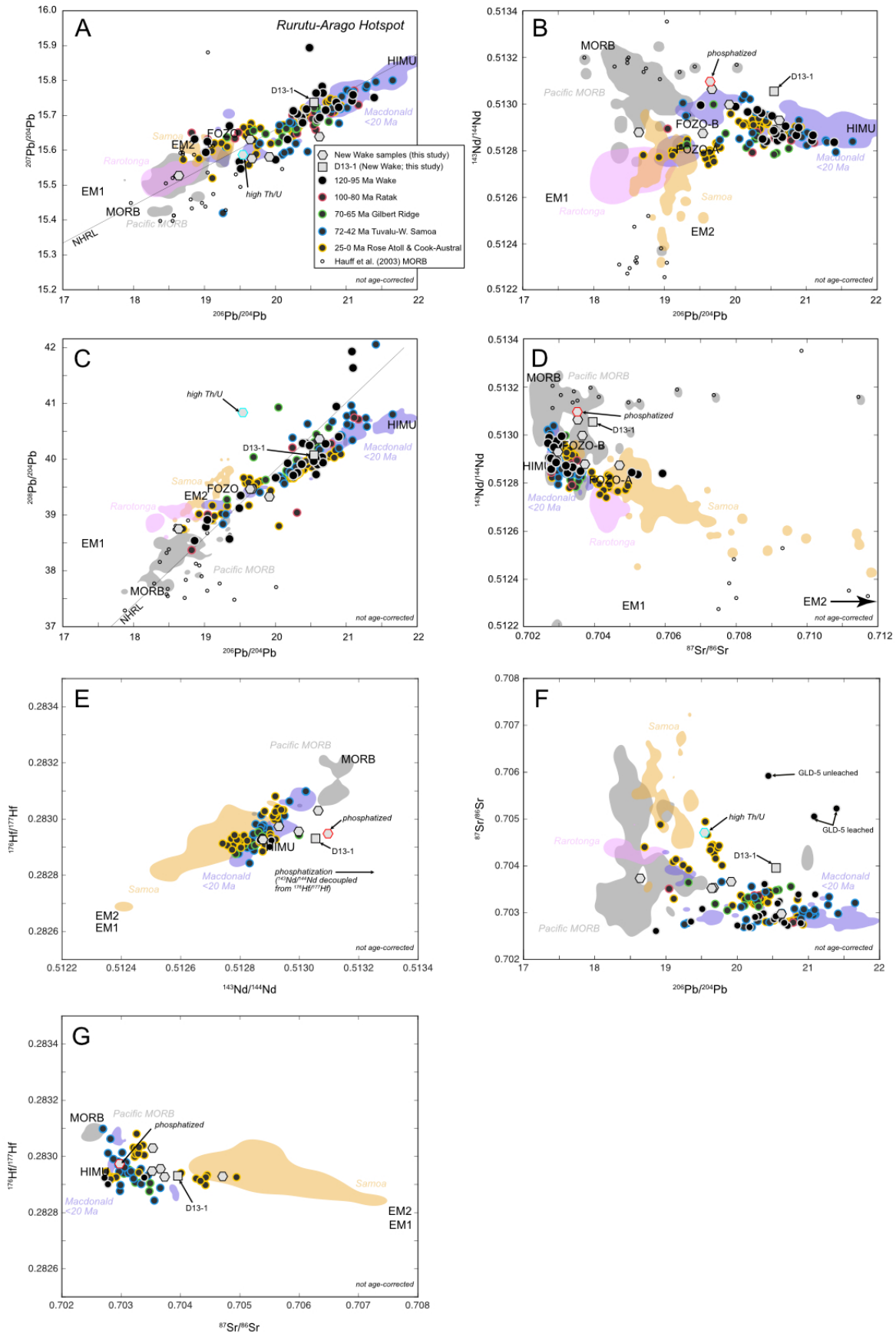


1115
1116
1117
1118
1119
1120
1121
1122

Extended Data Figure 6. Rotation (Euler) pole modeling is accomplished by a grid search for the best-fit pole (0.7°S , 315.7°E), shown as the latitude-longitude location for which the minimum misfit is found (white dot). Constraints for the modeled rotation are the colored seamount locations (blue and red, selected based on their apparent fit in composition), and the approximate age range for these volcanic tracks (80 -100 Ma), based on model-specific, new, and adjacent seamount volcanic ages^{29,68}

This is a preprint of an article that has been submitted to Nature, and revised based on two rounds of peer review, but has yet to be formally accepted for publication.

1123 *(black numbers next to seamount markers). Only two samples from EX1606 had material suitable for*
1124 *age dating, but four of the samples were attempted. Two succeeded, with one yielding a 91.3 Ma age*
1125 *that confirms that the Rurutu-Arago plume was active in the Wake region. The second successful*
1126 *sample predates passage of this area of the Pacific crust over the Rurutu-Arago hotspot and is*
1127 *excluded as a constraint on the modified stage pole. The two unsuccessful samples lacked a*
1128 *statistically robust plateau and were therefore inconclusive. Open circles represent Wake area*
1129 *seamounts and their ages, predating the 80 – 100 Ma time period modeled.*
1130

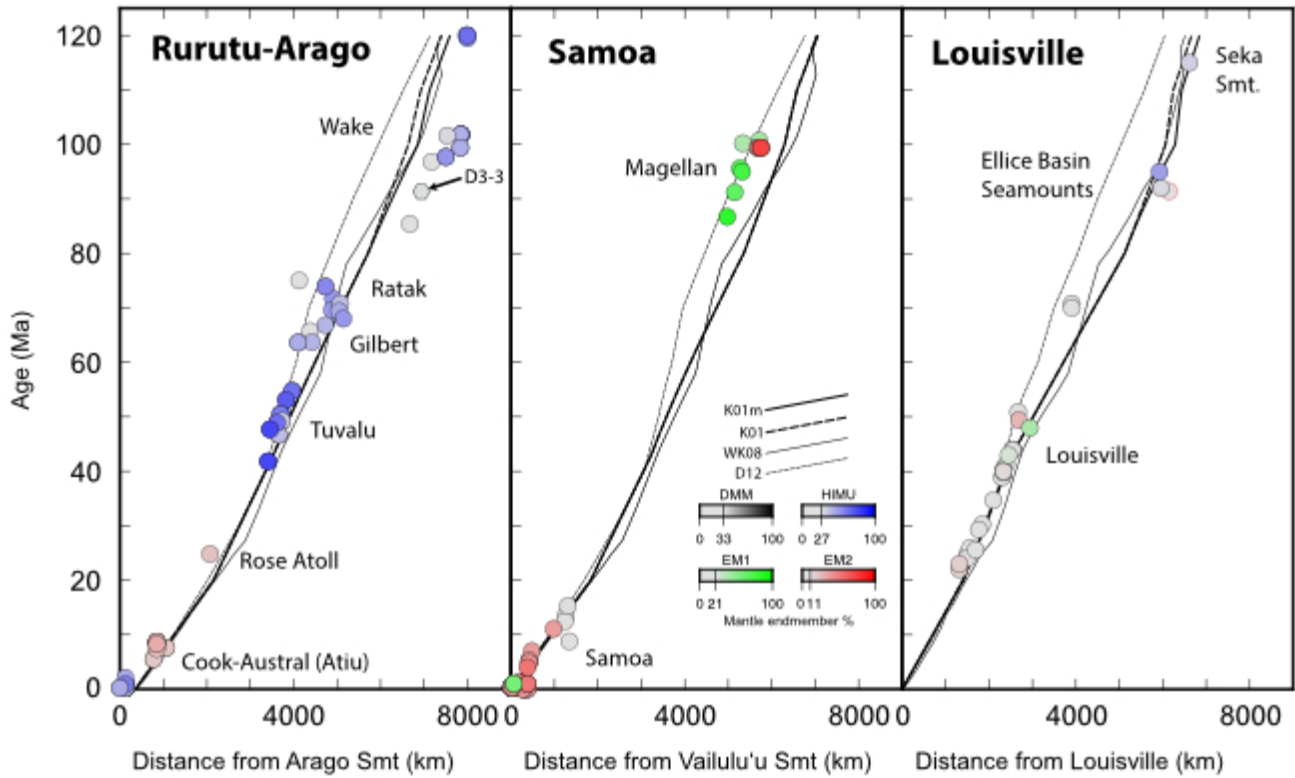


1132

1133 **Extended Data Figure 7.** Non-age-corrected plots of **A)** $^{207}\text{Pb}/^{204}\text{Pb}$ vs. $^{206}\text{Pb}/^{204}\text{Pb}$, **B)** $^{143}\text{Nd}/^{144}\text{Nd}$ vs.
1134 $^{206}\text{Pb}/^{204}\text{Pb}$, **C)** $^{208}\text{Pb}/^{204}\text{Pb}$ vs. $^{206}\text{Pb}/^{204}\text{Pb}$, **D)** $^{143}\text{Nd}/^{144}\text{Nd}$ vs. $^{87}\text{Sr}/^{86}\text{Sr}$, **E)** $^{143}\text{Nd}/^{144}\text{Nd}$ vs. $^{176}\text{Hf}/^{177}\text{Hf}$,
1135 **F)** $^{206}\text{Pb}/^{204}\text{Pb}$ vs. $^{87}\text{Sr}/^{86}\text{Sr}$, and **G)** $^{87}\text{Sr}/^{86}\text{Sr}$ vs. $^{176}\text{Hf}/^{177}\text{Hf}$ of our new Wake seamount samples
1136 (hexagons) compared to published data for the Tuvalu, Gilbert Ridge, Marshall/Ratak, and Wake
1137 Seamount portions of the Rurutu-Arago track (circles). Background data for young segments of the
1138 Cook-Austral plumes (Macdonald, Rurutu-Arago, Rarotonga), the Samoan plume, and Pacific MORB
1139 are given as 2σ contours of kernel density estimates (KDEs) of their respective datasets. Rarotonga
1140 lacks enough overlapping Sr, Pb, and Hf isotope data to be shown in panels **E** and **G**. Jurassic Pacific
1141 MORB data with seawater U alteration¹⁰¹ is also shown as small black open circles as a reference for
1142 how Pb isotopes may be disrupted in old seafloor basalts – and which is not evident in our new Wake
1143 samples (panels **A-D**). A 2σ contour of the KDE for published Wake seamounts is shown as an open
1144 grey contour. In both plots, the new Wake data plots within the known compositional range for the
1145 Wake Seamounts and the greater extent of the track. One of the new samples (outlined in cyan in
1146 panels **A-C, F**) has unusually high $^{208}\text{Pb}/^{204}\text{Pb}$; this is a signature occasionally expressed in older
1147 Rurutu-Arago lavas and persists after strong leaching¹⁴¹⁴. Here, $^{208}\text{Pb}/^{204}\text{Pb}$ is positively correlated
1148 with Th/U (see Extended Data Figure 10), indicating U loss during alteration. Data are not corrected
1149 for post-eruptive radiogenic ingrowth (see Methods). We also identify a clear phosphatization
1150 signature (high Y/Y*; see Supplementary Data Table 1) in another of the new Wake samples (outlined
1151 in red in panels **B, D, and G**). As discussed in detail in the Supplement, strongly leached samples that
1152 have undergone significant phosphatization tend to have highly radiogenic $^{143}\text{Nd}/^{144}\text{Nd}$ of unclear
1153 origin. In such samples, Nd isotopes decouple from Sr isotopes (panel **D**) and Hf isotopes (panel **E**);
1154 obscuring some source mantle information. Here, $^{87}\text{Sr}/^{86}\text{Sr}$ vs. $^{176}\text{Hf}/^{177}\text{Hf}$ provide a more useful
1155 “isotopic fingerprint” of the HIMU-to-FOZO provenance characteristic of other Rurutu-Arago
1156 seamounts than plots using $^{143}\text{Nd}/^{144}\text{Nd}$, and are consistent with interpretations from the Pb isotopes.

1157

1158

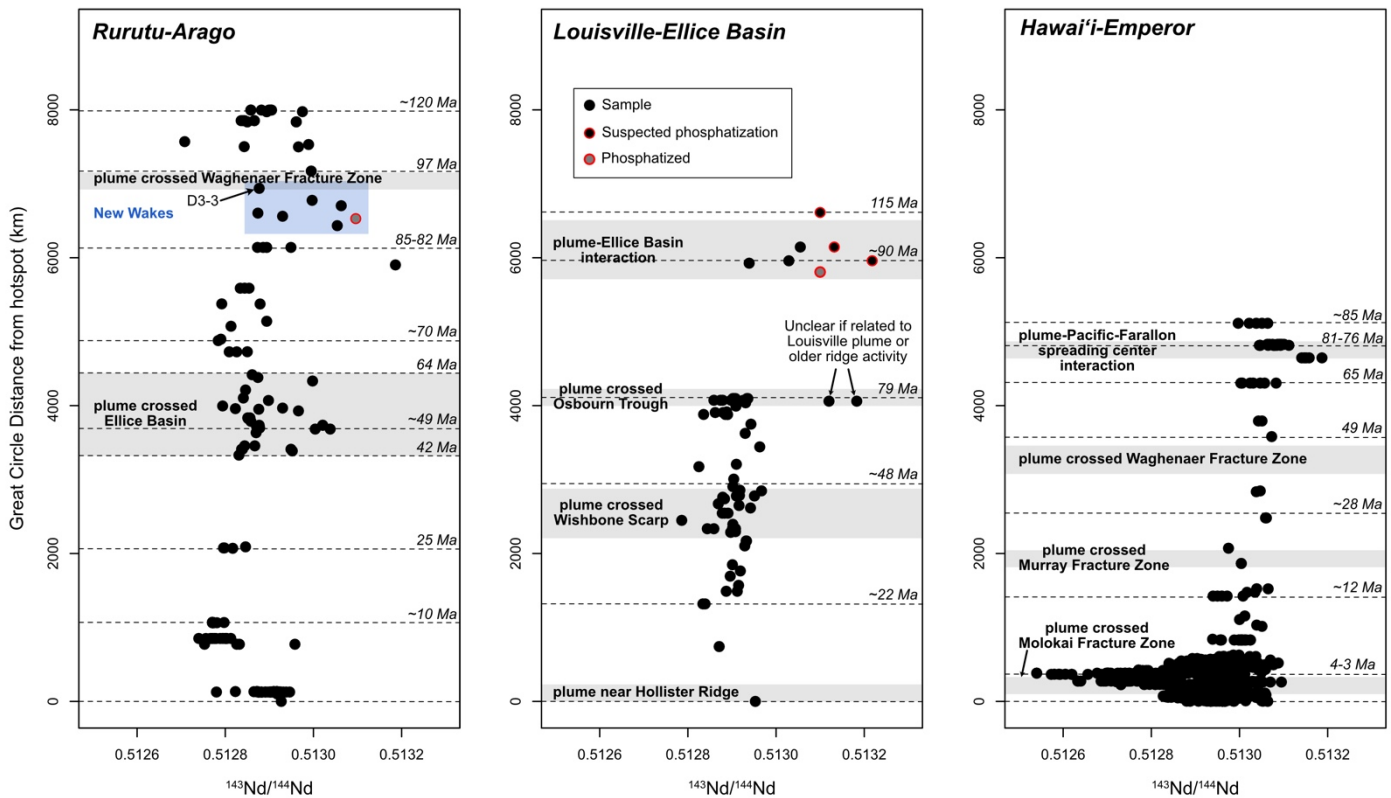


1159

1160

1161 **Extended data Figure 8.** Age-distance relationships of the Rurutu-Arago, Samoan, Louisville,
1162 plumes (see Background Data Sources For Figures in Methods). Data shown here are only samples
1163 with age determinations or published age estimates (where well constrained by nearby volcanoes^{14,28}
1164 and Sr-Pb-Nd data to permit color coding. APM models are also included for reference (WK08³⁹ =
1165 Wessel and Kroenke, 2008; D12⁶ = Doubrovine et al., 2012 without plume drift correction; K01¹⁸ =
1166 Koppers et al., 2001; K01m = modified Koppers et al., 2001 from this study). The oldest portions of the
1167 Hotspot Highway are in good agreement with K01m model predictions; some scatter occurs as a
1168 function of plume drift (e.g., Cretaceous portion of the Samoa hotspot; see Extended Data Figure 5).
1169 For the hotspots shown here, the data are consistent with age progressions that can be traced back into
1170 the Cretaceous, including the successful 91.3 Ma age determination from our new sample set. Rurutu-
1171 Arago has HIMU to FOZO-like compositions, while Samoan volcanoes are EM-type to FOZO in
1172 composition. The Rurutu-Arago age progression can be clearly traced into the Wakes and back to
1173 ~120 Ma. The Samoan plume was active during the Cretaceous, forming the Magellan chain in the
1174 West Pacific where EM2 and EM1 compositions consistent with those found in Samoan shield and

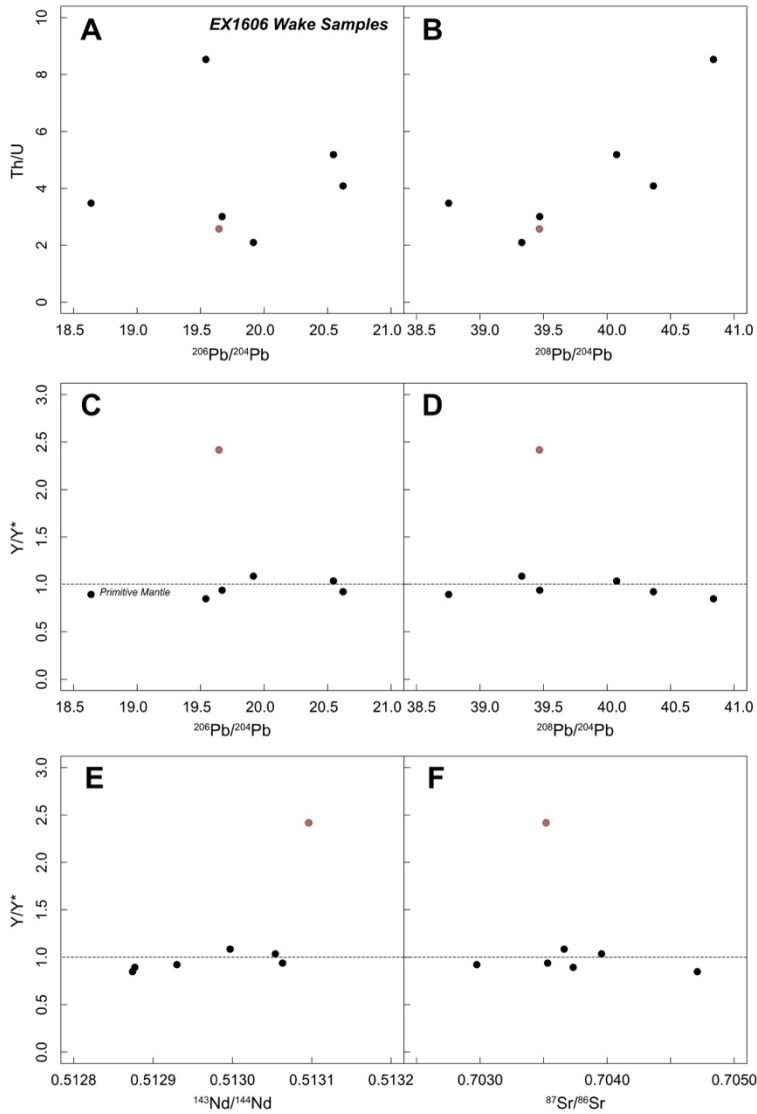
rejuvenated volcanoes, respectively (see Extended Data Figure 3 for details). The FOZO Louisville hotspot track and older Ellice Basin Seamounts as well as Seka Seamount; which are likely FOZO-to-DMMLike with Pb isotopes partly overprinted by seawater U ingrowth, are also age-progressive.



Extended Data Figure 9. Great circle distance (km) from active hotspot center vs. $^{143}\text{Nd}/^{144}\text{Nd}$ (not age-corrected) for the (left) Rurutu-Arago, (center) Louisville-Ellice Basin Seamounts, and (right) Hawai'i-Emperor hotspot tracks. Isochrons are provided as dashed lines, and light grey fields mark where the plumes interacted with ridges or fracture zones. All three hotspot tracks record significant variability in isotopic composition over time that correspond to interaction of the plume with major lithospheric structural features. Rurutu-Arago, which was a true-intraplate hotspot for the entirety of its documented history, produced episodes of depleted (high $^{143}\text{Nd}/^{144}\text{Nd}$) melts that coincide spatially with major lithospheric structures, but otherwise maintains a fairly constant $^{143}\text{Nd}/^{144}\text{Nd}$ over time. Samples with evidence of phosphatization (high Y/Y^* and/or P_2O_5 ; see Extended Data Figure 10) are shown as light grey circles with red outlines. Black circles with red outlines are samples that may have been phosphatized ($^{143}\text{Nd}/^{144}\text{Nd} > \sim 0.5131$) but cannot be confirmed due to lack of available major and

1192 *trace element data. By contrast, the Louisville hotspot track, including the Ellice Basin Seamounts,*
1193 *records a long-term trend of enrichment with time that records its transition from plume-ridge*
1194 *interaction to true intraplate. Deviations also occur when the plume crossed the Osbourn Trough*
1195 *(however, it remains unclear whether this is related to the Louisville plume), and later the Wishbone*
1196 *Scarp (attributed to source mantle heterogeneity^{28,103}). The broad enrichment trend in Louisville is*
1197 *similar to long-term enrichment observed in the Hawaiian plume, which also interacted with a ridge in*
1198 *the Cretaceous before transitioning to a true-intraplate plume system⁹⁹. Data sources are the same as*
1199 *in Fig. 1.*
1200

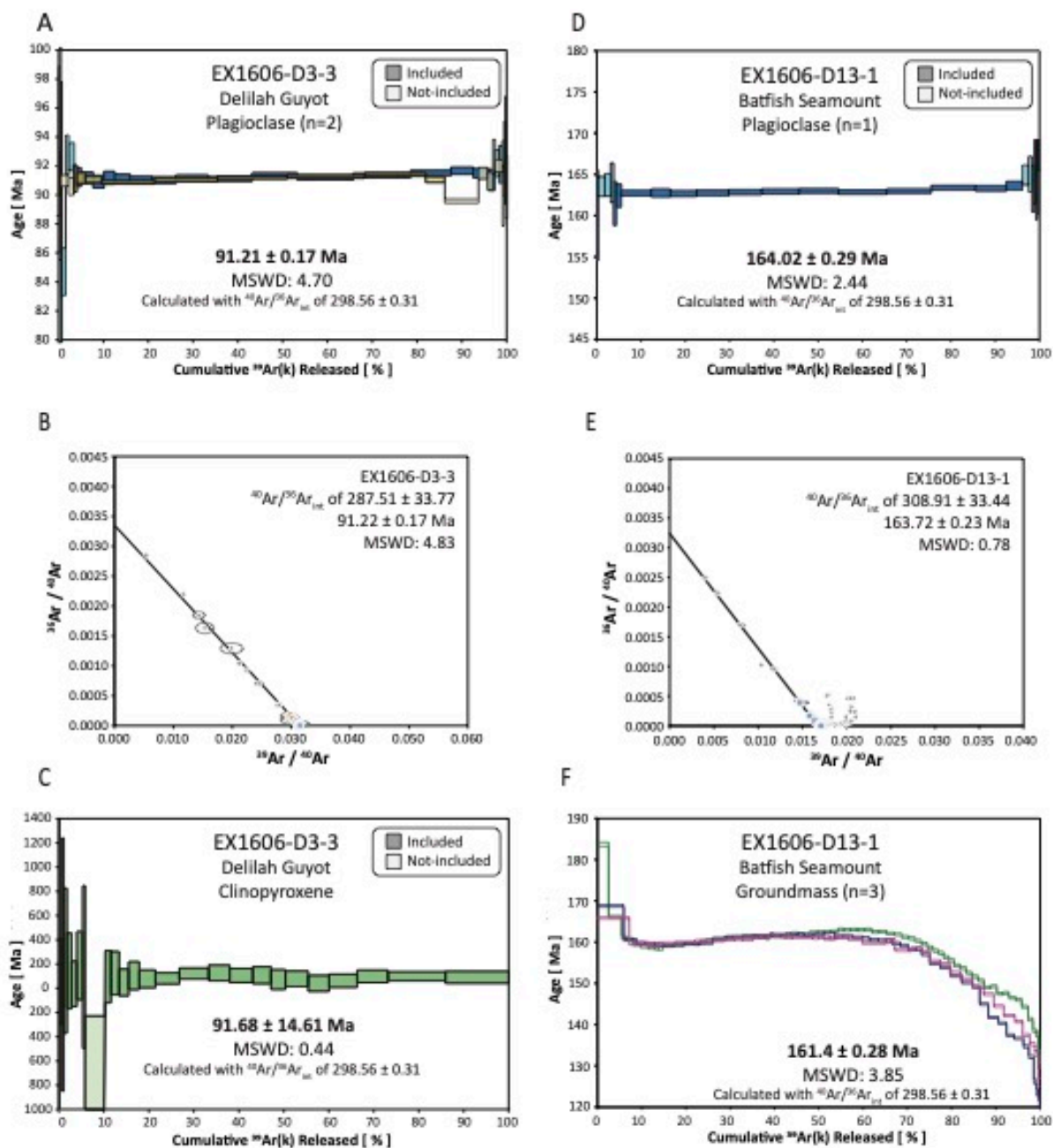
1201



1202

1203 **Extended Data Figure 10.** Trace element alteration proxies versus Sr-Nd-Pb isotope compositions of
1204 the new Wakes (EX1606) samples. **A)** Th/U versus measured $^{206}\text{Pb}/^{204}\text{Pb}$, **B)** Th/U versus measured
1205 $^{208}\text{Pb}/^{204}\text{Pb}$, and **C-F)** Y/Y* versus radiogenic isotope compositions. Versus Th/U, $^{206}\text{Pb}/^{204}\text{Pb}$ (**A**)
1206 exhibits only a weak correlation with Th/U, while $^{208}\text{Pb}/^{204}\text{Pb}$ (**B**) is much more strongly correlated,
1207 indicating modification of U abundances in the EX1606 samples. $^{143}\text{Nd}/^{144}\text{Nd}$ (**E**) exhibits some
1208 correlation versus Y/Y*, a proxy for phosphatization, becoming more radiogenic at high Y/Y*, while
1209 Pb and Sr isotopes show no correlation.

1210



1211

1212 **Extended Data Figure 11.** $^{40}\text{Ar}/^{39}\text{Ar}$ Age determinations for EX1606-D3-3 and EX1606-D13-1. A)
 1213 Stacked EX1606-D3-3 age plateau from plagioclase separates for Batfish Seamount (n=2). Included
 1214 steps are shown in dark blue and dark yellow, and not included steps are shown in light blue and light
 1215 yellow. B) Inverse Isochron for EX1606-D3-3 plagioclase separates (n=2). Included steps are shown
 1216 in blue and yellow, and not included steps are shown in grey. The solid line indicates the measured
 1217 $^{40}\text{Ar}/^{36}\text{Ar}$ initial ratios. C) EX1606-D3-3 age plateau from a clinopyroxene separate. Included steps are

1218 *shown in dark green, and not-included steps are shown in light green. D) EX1606-D13-1 age plateau*
1219 *from plagioclase separates at Unnamed Seamount (n=1). Included steps are shown in dark blue and*
1220 *not-included steps are shown in light blue. E) Inverse isochron for EX1606-D13-1 for groundmass and*
1221 *plagioclase separates (n=4). Included steps are shown in blue, and not included steps are shown in*
1222 *grey. The solid line indicates the measured $^{40}\text{Ar}/^{36}\text{Ar}$ initial ratios F) Stacked EX1606-D13-1 age*
1223 *plateau determinations for groundmass separates. None of the groundmass experiments produced a*
1224 *concordant age determination.*

1225

1226

1227
1228

Extended Data Table 1 . Stage poles for the Modified Pacific Hotspot Reference Frame Absolute Plate Motion Model (italics from K01¹⁸)

Stage start (Ma)	Stage end (Ma)	Latitude (°N)	Longitude (°E)	Rotation Rate (°/Myr)	Standard Deviation
<i>0</i>	<i>20</i>	<i>70.1</i>	<i>302.0</i>	<i>0.88</i>	<i>0.016</i>
<i>20</i>	<i>43</i>	<i>67.1</i>	<i>294.5</i>	<i>0.58</i>	<i>Not given</i>
<i>43</i>	<i>80</i>	<i>18.8</i>	<i>253.6</i>	<i>0.66</i>	<i>0.029</i>
<i>80</i>	<i>100</i>	<i>-0.7</i>	<i>315 .7</i>	<i>0.97</i>	<i>5</i> <i>0.06</i>
<i>100</i>	<i>110</i>	<i>75.1</i>	<i>44.8</i>	<i>0.44</i>	<i>Not given</i>
<i>110</i>	<i>125</i>	<i>65.3</i>	<i>273.2</i>	<i>0.45</i>	<i>0.042</i>

1229
1230

Extended Data Table 2. Locations used to constrain the revised 100-80 Ma stage pole.

	Latitude (°N)	Longitude (°E)
Magellan Seamounts:		
1	20.17	151.53
2	19.48	151.57
3	19.55	151.57
4	20.1	151.57
5	19.88	151.9
6	19.37	151.97
7	17.03	154.07
8	17.2	154.33
9	16.4	154.35
10	15.5	155.02
11	15.88	155.15
12	14.13	155.88
13	14.18	155.98
14	14.17	156
15	12.98	156.68
16	12.97	156.75
Marshall Seamounts:		
17	20.45	163.72
18	19.15	164.56
19	19.45	165.8
20	17.31	165.96
21	18.32	165.98
22	18.47	166.68
23	13.9	167.65
24	8.76	169.79

1231

1232

1233

1234